


Article

# Hydration and Ion Pair Formation in Aqueous Lu<sup>3+</sup>- Solution

Wolfram Rudolph <sup>1,\*</sup>  and Gert Irmer <sup>2</sup>

<sup>1</sup> Medizinische Fakultät der TU Dresden, Institut für Virologie im MTZ, Fiedlerstr. 42, 01307 Dresden, Germany

<sup>2</sup> Technische Universität Bergakademie Freiberg, Institut für Theoretische Physik, Leipziger Str. 23, 09596 Freiberg, Germany; irmer@physik.tu-freiberg.de

\* Correspondence: Wolfram.Rudolph@tu-dresden.de; Tel.: +49-351-458-6200

Received: 19 November 2018; Accepted: 3 December 2018; Published: 7 December 2018



**Abstract:** Aqueous solutions of Lu<sup>3+</sup>- perchlorate, triflate and chloride were measured by Raman spectroscopy. A weak, isotropic mode at 396 cm<sup>-1</sup> (full width at half height (fwhh) at 50 cm<sup>-1</sup>) was observed in perchlorate and triflate solutions. This mode was assigned to the totally symmetric stretching mode of [Lu(OH<sub>2</sub>)<sub>8</sub>]<sup>3+</sup>,  $\nu_1$ LuO<sub>8</sub>. In Lu(ClO<sub>4</sub>)<sub>3</sub> solutions in heavy water, the  $\nu_1$ LuO<sub>8</sub> symmetric stretch of [Lu(OD<sub>2</sub>)<sub>8</sub>]<sup>3+</sup> appears at 376.5 cm<sup>-1</sup>. The shift confirms the theoretical isotopic effect of this mode. In the anisotropic scattering of aqueous Lu(ClO<sub>4</sub>)<sub>3</sub>, five bands of very low intensity were observed at 113 cm<sup>-1</sup>, 161.6 cm<sup>-1</sup>, 231 cm<sup>-1</sup>, 261.3 cm<sup>-1</sup> and 344 cm<sup>-1</sup>. In LuCl<sub>3</sub> (aq) solutions measured over a concentration range from 0.105–3.199 mol·L<sup>-1</sup> a 1:1 chloro-complex was detected. Its equilibrium concentration, however, disappeared rapidly with dilution and vanished at a concentration < 0.5 mol·L<sup>-1</sup>. Quantitative Raman spectroscopy allowed the detection of the fractions of [Lu(OH<sub>2</sub>)<sub>8</sub>]<sup>3+</sup>, the fully hydrated species and the mono-chloro complex, [Lu(OH<sub>2</sub>)<sub>7</sub>Cl]<sup>2+</sup>. In a ternary LuCl<sub>3</sub>/HCl solution, a mixture of chloro-complex species of the type [Lu(OH<sub>2</sub>)<sub>8-n</sub>Cl<sub>n</sub>]<sup>+3-n</sup> (*n* = 1 and 2) were detected. DFT geometry optimization and frequency calculations are reported for Lu<sup>3+</sup>- water cluster in vacuo and with a polarizable dielectric continuum (PC) model including the bulk solvent implicitly. The bond distance and angle for [Lu(OH<sub>2</sub>)<sub>8</sub>]<sup>3+</sup> within the PC are in good agreement with data from structural experiments. The DFT frequencies for the Lu-O modes of [Lu(OH<sub>2</sub>)<sub>8</sub>]<sup>3+</sup> and its deuterated analog [Lu(OD<sub>2</sub>)<sub>8</sub>]<sup>3+</sup> in a PC are in fair agreement with the experimental ones. The calculated hydration enthalpy of Lu<sup>3+</sup> (aq) is slightly lower than the experimental value.

**Keywords:** Raman spectroscopy; Lu(ClO<sub>4</sub>)<sub>3</sub>; Lu(CF<sub>3</sub>SO<sub>3</sub>)<sub>3</sub> and LuCl<sub>3</sub> solutions in H<sub>2</sub>O and D<sub>2</sub>O; Lu<sup>3+</sup>- hydration; Lu-O skeleton modes; monochloro complex of Lu<sup>3+</sup>; DFT calculations of [Lu(OH<sub>2</sub>)<sub>8</sub>]<sup>3+</sup>; polarizable dielectric continuum model

## 1. Introduction

The element lutetium (Lu), a silvery white metal with the atomic number 71, is the heaviest of the lanthanides and has a full f-electron shell with a configuration: [Xe] 4f<sup>14</sup>5d<sup>1</sup>6s<sup>2</sup>. With a crustal abundance of 0.32 ppm [1,2], it is one of the rarest of the lanthanides. Because of this rarity and accompanying high price, only a few applications of this metal are known to date. Lutetium is used as a catalyst for cracking hydrocarbons in oil refineries [3,4]. Lutetium aluminum garnet (LuAG, Lu<sub>3</sub>Al<sub>5</sub>O<sub>12</sub>) is primarily known for its use in high-efficiency laser devices [5]. Lutetium oxyorthosilicat (LSO), a silicon oxygen compound of lutetium doped with cerium, is utilized as a detector for positron emission tomography [6]. Naturally occurring lutetium comprises two isotopes: <sup>175</sup>Lu and <sup>176</sup>Lu. <sup>176</sup>Lu is unstable with an extremely long half-life of 3.78 × 10<sup>10</sup> years which makes it suitable for

determining the age of meteorites [7]. A short lived radionuclide  $^{177}\text{Lu}$  (half-life of 6.6430 days [8]) is used in the treatment of certain tumors, mainly neuroendocrine tumors [9].

In aqueous solution, lutetium exists exclusively in the trivalent state,  $\text{Lu}^{3+}$ , and is strongly hydrated due to its high charge to radius ratio. Trivalent lutetium has the smallest ionic radius of all 15 lanthanides ( $\text{Ln}^{3+}$ ) across the series from lanthanum to lutetium known as the lanthanide contraction.  $\text{Lu}^{3+}$  hydrolyses most, i.e. shows a lesser basicity, than the preceding trivalent rare earth ions in aqueous solution. The difference in basicity is the basis for all separation methods of the individual rare earth ions [10]. The hydrolysis constant for the first monomeric species,  $\beta_1^\circ$  at 25 °C for  $\text{LuOH}^{2+}$  is  $4.677 \times 10^{-8}$ , the largest across the series, while for  $\text{LaOH}^{2+}$ , the lowest, it is  $1.288 \times 10^{-9}$  [11]. However, compared to other trivalent metal ions such as  $\text{Al}^{3+}$  or  $\text{Fe}^{3+}$ , the hydrolysis is much less pronounced.

Light rare earth ions are nonahydrates while the heavy rare earth ions are octahydrates in aqueous solution with weakly complex forming anions. The crossover of the hydration number from 9 to 8 occurs in the middle of the series. This sudden change in hydration number, known as *gadolinium break*, was used to explain experimental data in aqueous solution [12–15]. Recent studies, however, concluded that no such break exists and that the hydration number of  $\text{Ln}^{3+}$  ions smoothly changes from 9 to 8 across the series [16–18] with the rare earth (RE) ions of the series having non-integer numbers between 9 and 8 in the middle of the series. This means that the water ligands in the nona-/octahydrates exchange rapidly with each another [19,20].

For the  $\text{Lu}^{3+}$  ion in aqueous solution, the local hydration structure was measured using extended X-ray absorption fine structure (EXAFS) spectroscopy [16,21–24] and X-ray diffraction [25,26]. The majority of studies agreed with the 8-fold coordination of water molecules grouped around  $\text{Lu}^{3+}$  in square antiprismatic (SAP) geometry. A combined study using molecular dynamics (MD) simulation and EXAFS measurement proved the SAP structure of the  $\text{Lu}^{3+}$ -octahydrate and the  $\text{Lu}^{3+}$ -O bond distance was given at 2.32 Å [21].

The reported Lu-O bond distances range from 2.282 Å to 2.35 Å. These variations may be due to the fact that XRD measured concentrated solutions while EXAFS used relatively dilute solutions [16,21]. However, such differences in concentration scale, pose a problem because ion pairs are likely to form in concentrated solutions [26–29]. Ion association studied on these solutions do not agree on the nature of the ion pairs/complex species formed. In addition to the detected complex species, there is no doubt that outer-sphere and outer-outer sphere ion pairs exist in rare earth solutions. A recent dielectric relaxation spectroscopy (DRS) study on chloride, nitrate and sulfate solutions of  $\text{La}^{3+}$  and  $\text{Eu}^{3+}$  claimed, exclusively, outer-sphere and outer-outer-sphere ion pairs in these solutions [30]. However, in a variety of studies applying a wide array of methods such as solvent extraction [31–34], ion exchange [35–37], fluorescence spectroscopy [38–40], ultrasound absorption [41–44] and NMR spectroscopy [45–47], it was convincingly shown that complex species also exist in aqueous solution contrary to the new DRS results [30] put forward.

Raman spectroscopy probes the immediate environment of metal ions in solution and was frequently used to study hydrated metal ions and ion association. RE-ions, however, have only recently been measured at a sufficiently high quality in the low frequency region of the Raman spectrum. These spectra then allow the construction of the isotropic scattering profile from the measured data. A highly polarized band in the low frequency region of the Raman spectrum due to the symmetrical metal-oxygen mode of the hydrated cations is the most characteristic peak [26–29,48–51]. This mode is sensitive to possible ion pair formation. Occasionally, all the theoretically predicted bands of the metal-oxygen modes may be observed and used to support the assignment of the point group symmetry and the coordination number in these aqueous solutions. Raman scattering measurements on  $\text{Lu}^{3+}$  (aq) should allow, in principle, the characterization of the solution structure in greater detail. No systematic Raman studies on aqueous lutetium solutions exist but one study on a glassy  $\text{LuCl}_3$  (aq) sample at high concentrations was reported [52].

The present study was undertaken to characterize the hydration and speciation in aqueous  $\text{Lu}^{3+}$  solutions and to this end  $\text{Lu}^{3+}$ -salt solutions with common anions ( $\text{ClO}_4^-$ ,  $\text{CF}_3\text{SO}_3^-$  and  $\text{Cl}^-$ ) were considered over a broad concentration range and down to the low frequency region. Triflate (trifluoromethanesulfonate) and perchlorate are considered weakly-complex-forming anions and were, therefore, chosen to measure the Lu-O stretching modes in aqueous solution so as to identify and assign bands unique to the first hydration sphere of  $\text{Lu}^{3+}$  (aq). A  $\text{Lu}(\text{ClO}_4)_3$  solution in heavy water was also measured to characterize the vibrational isotope effect by changing from  $[\text{Lu}(\text{H}_2\text{O})_8]^{3+}$  to  $[\text{Lu}(\text{D}_2\text{O})_8]^{3+}$ . In a variety of di- and trivalent metal ion solutions with chloride as counterion, however, it has been shown that these anions readily form complexes [27–29] and the question arises as to whether chloro-complex species occur in  $\text{Lu}^{3+}$  (aq) solutions. A  $\text{LuCl}_3$  solution series and a ternary solution of  $\text{LuCl}_3/\text{HCl}$  were studied in order to answer the question whether chloro-complex species exist and if possible to quantify the fraction of the chloro-complex species.

In addition, simulations on lutetium-water species with eight water molecules were considered by applying density functional theory (DFT) in the gas phase. Furthermore, the  $\text{Lu}^{3+}$ -species with a polarizable dielectric continuum were also simulated in order to take into account the effects of the bulk solvent. Frequency calculations were carried out via the calculation of the second derivative of the energy with respect to the nuclear positions of the optimized  $\text{Lu}^{3+}$ -water species. Furthermore, the hydration enthalpy of the  $\text{Lu}^{3+}$  ion at 25 °C was modeled.

## 2. Experimental Details; Data Analysis and DFT Calculations on $\text{Lu}^{3+}$ -Water Hydrates

### 2.1. Preparation of Solutions

Lutetium stock solutions were prepared and the lutetium concentrations of these solutions were analysed by complexometric titration [53]. The solution densities were determined with a pycnometer at 23 °C and the molar ratios of water per salt were calculated ( $R_w$ -values). For Raman spectroscopic measurements, the solutions were filtered through a fine sintered glass frit (1–1.6  $\mu\text{m}$  pore size). The solutions showed no Tyndall effect and were “optically empty” [54].

Lutetium perchlorate solutions were prepared from  $\text{Lu}_2\text{O}_3$  (99.9%, Merck KGaA, Darmstadt, Germany) and  $\text{HClO}_4$  in a beaker until all oxide dissolved. A  $\text{Lu}(\text{ClO}_4)_3$  stock solution was prepared at  $2.233 \text{ mol}\cdot\text{L}^{-1}$  ( $R_w = 19.01$ ). The slightly acidified solution using  $\text{HClO}_4$  had a pH value at  $\sim 1.0$ . From this stock solution, three dilute solutions were prepared:  $1.132 \text{ mol}\cdot\text{L}^{-1}$  ( $R_w = 42.77$ ),  $0.556 \text{ mol}\cdot\text{L}^{-1}$  ( $R_w = 92.40$ ), and  $0.186 \text{ mol}\cdot\text{L}^{-1}$  ( $R_w = 289.0$ ). The solutions were analyzed for dissolved chloride with a 5%  $\text{AgNO}_3$  solution. The absence of a white  $\text{AgCl}$  precipitate was proof that the stock solution was free of  $\text{Cl}^-$ .

Two  $\text{Lu}(\text{ClO}_4)_3$  solutions in heavy water were prepared from a deuterated  $\text{Lu}(\text{ClO}_4)_3$  stock solution and with 99.9 atom % D (Sigma-Aldrich) at  $1.398 \text{ mol}\cdot\text{L}^{-1}$  and  $0.439 \text{ mol}\cdot\text{L}^{-1}$ . The deuteration degree of the  $0.439 \text{ mol}\cdot\text{L}^{-1}$   $\text{Lu}(\text{ClO}_4)_3$  solution in  $\text{D}_2\text{O}$  was better than 97% D.

A  $1.05 \text{ mol}\cdot\text{L}^{-1}$   $\text{Lu}(\text{CF}_3\text{SO}_3)_3$  solution prepared from anhydrous  $\text{Lu}(\text{CF}_3\text{SO}_3)_3$  (99.9%, Sigma-Aldrich,) and triply distilled water. The solution had a pH value at  $\sim 1.0$ .

A stock solution of  $\text{LuCl}_3$  at  $3.199 \text{ mol}\cdot\text{L}^{-1}$  ( $R_w = 15.68$ ) was prepared from  $\text{Lu}_2\text{O}_3$  (99.9%, Sigma-Aldrich,) and  $\text{HCl}$  in a beaker covered with a glass lid until all oxide dissolved. The pH value of the stock solution was 0.85. The following solutions were prepared from the stock solution and triply distilled water by weight:  $1.890 \text{ mol}\cdot\text{L}^{-1}$  ( $R_w = 28.51$ ),  $0.935 \text{ mol}\cdot\text{L}^{-1}$  ( $R_w = 59.00$ ),  $0.478 \text{ mol}\cdot\text{L}^{-1}$  ( $R_w = 115.99$ ),  $0.241 \text{ mol}\cdot\text{L}^{-1}$  ( $R_w = 229.86$ ) and  $0.105 \text{ mol}\cdot\text{L}^{-1}$  ( $R_w = 528.65$ ). Furthermore, a solution with an excess of  $\text{HCl}$  (37%, zur Analyse, Merck KGaA, Darmstadt, Germany) was prepared from the  $\text{LuCl}_3$  stock solution and a 37%  $\text{HCl}$  solution (37%, zur Analyse, Merck, Darmstadt, Germany) by weight. The ternary solution contained  $1.589 \text{ mol}\cdot\text{L}^{-1}$   $\text{LuCl}_3$  and  $6.047 \text{ mol}\cdot\text{L}^{-1}$   $\text{HCl}$ . An  $\text{HCl}$  solution was also prepared at  $6.04 \text{ mol}\cdot\text{L}^{-1}$  from a 37%  $\text{HCl}$  solution.

## 2.2. Spectroscopic Measurements:

Raman spectra were measured in the macro chamber of the T 64000 Raman spectrometer from Jobin Yvon in a 90° scattering geometry at 23 °C. These measurements have been described elsewhere [49,55]. A quartz cuvette from Hellma Analytics (Müllheim, Germany) with 10 mm path length and a volume 1000 µL was used. Briefly, the spectra were excited with the 487.987 nm line of an Ar<sup>+</sup> laser at a power level of 1100 mW at the sample. After passing the spectrometer in subtractive mode, with gratings of 1800 grooves/mm, the scattered light was detected with a cooled CCD detector. The scattering geometries I<sub>VV</sub> = (X[ZZ]Y) and I<sub>VH</sub> = (X[ZX]Y) are defined as follows: the propagation (wave vector direction) of the exciting laser beam is in X direction and the propagation of the observed scattered light is in Y direction, the 90° geometry. The polarisation (electrical field vector) of the laser beam is fixed in Z direction (vertical) and the polarisation of the observed scattered light is observed in Z direction (vertical) for the I<sub>VV</sub> scattering geometry. For I<sub>VH</sub> the fixed electric field vector of the exciting laser beam in Z direction (vertical) and the observed scattering light is polarized in the X direction (horizontal). Thus, for the two scattering geometries it follows:

$$I_{VV} = I(X[ZZ]Y) = 45\bar{\alpha}'^2 + 4\gamma'^2 \quad (1)$$

$$I_{VH} = I(X[ZX]Y) = 3\gamma'^2 \quad (2)$$

The symbols  $\bar{\alpha}'$  and  $\gamma'$  are the isotropic and the anisotropic invariant of the Raman polarizability tensor, respectively [49,55]. The isotropic spectrum, I<sub>iso</sub> was constructed according to Equation (3):

$$I_{iso} = I_{VV} - 4/3 \times I_{VH} \quad (3)$$

The polarization degree of the Raman bands,  $\rho$  ( $\rho = I_{VH}/I_{VV}$ ) was determined using an analyzer and adjusted, if necessary, before each measuring cycle using CCl<sub>4</sub>. A detailed account of this procedure may be found in ref [49,55].

In order to characterize the spectral features in the low wavenumber region, the Raman spectra in I-format were reduced and the R-spectra obtained. The R-spectra have been constructed according to the procedure previously described [49]. The I-spectra were corrected for the scattering factor  $(\nu_L - \bar{\nu})^3$  and further corrected for the Bose-Einstein temperature factor,  $B = [1 - \exp(-h\bar{\nu}c/kT)]$  and the frequency factor,  $\bar{\nu}$ , to give the so called reduced or R( $\bar{\nu}$ ) spectrum. The isotropic spectrum in R-format arise from the corrected R<sub>VV</sub> and R<sub>VH</sub> spectra according to Equation (4):

$$R(\bar{\nu})_{iso} = R(\bar{\nu})_{VV} - 4/3R(\bar{\nu})_{VH}. \quad (4)$$

In the low wavenumber region, the I( $\bar{\nu}$ ) and R( $\bar{\nu}$ ) spectra are significantly different and only the spectra in R-format are presented. It should be noted that one of the advantages of using isotropic R-spectra is that the baseline is almost flat in the 50–700 cm<sup>-1</sup> wavenumber region allowing relatively unperturbed observation of the presence of any weak modes [49,51].

## 2.3. Quantitative Raman Measurements

The quantitative relationship between the band intensity and the solute concentration by Raman measurements is the simple equation:  $I_i = J_i \times C_T$ , where  $I_i$  is the integrated band intensity of band  $i$  of the molecular species as a function of the scattering coefficient  $J_i$  multiplied by the solute concentration,  $C_T$  in mol·L<sup>-1</sup>. The perchlorate band in these solutions served as the internal standard. The result of the functional relationship between the integrated band intensity of the  $\nu_1$ LuO<sub>8</sub> mode in Lu(ClO<sub>4</sub>)<sub>3</sub> (aq) and the concentration of Lu<sup>3+</sup> (aq) is given by Equation (5):

$$I_{396} = 1148.3 \times C_T \quad (5)$$

The coefficient of determination,  $R^2$  is 0.99. The relationship holds if  $\text{Lu}(\text{ClO}_4)_3$  (aq) is completely dissociated into its ions and  $C_T$  is equal to the concentration of  $\text{Lu}^{3+}$ . The linearity of the integrated band intensity  $I_{396}$  versus solute concentration of  $\text{Lu}(\text{ClO}_4)_3$  up to a concentration at  $\sim 3 \text{ mol}\cdot\text{L}^{-1}$  proves this point. The  $\text{LuCl}_3$  solutions were then measured under the same conditions as the  $\text{Lu}(\text{ClO}_4)_3$  solutions and the integrated band intensities for the  $\nu_1 \text{LuO}_8$  mode could be determined and compared to the one in the perchlorate solution. The accuracy of the band intensities in these solutions was estimated to be  $\pm 5\%$ .

#### 2.4. DFT Calculations

The calculations were executed using the Gaussian03 package [56] employing the B3LYP functional [57]. The Stuttgart/Dresden (SDD) basis set was used which adequately reproduces the geometrical parameters, in particular the experimentally observed Lu–O distance. SDD uses a relativistic effective core potential (ECP) for  $\text{Lu}^{3+}$ . All electrons for the other atoms are described by Dunning/Huzinaga valence double-zeta (D95V) functions. Placing the octa-hydrate in a solvent continuum employing the Polarized Continuum Model (PCM) which takes into account the solvation effect of bulk water gave significantly better results compared with the experimental frequencies. The PCM used was the version described in ref. [58] where the solvent is modelled as an isotropic and homogeneous continuum, characterized by its dielectric properties. The cavity is defined as a set of interlocking spheres attached to the solute atoms. The electrostatic solute-solution interaction is calculated introducing an apparent charge distribution spread over the cavity surface.

Geometries of gas phase hydrates and within the PC framework with 8 water molecules surrounding the  $\text{Lu}^{3+}$  ion were optimized. The aqua ion with  $S_8$  symmetry was the only structure, which led to an energy minimum without imaginary frequencies. The geometrical data and the frequency of the breathing mode of the  $[\text{Lu}(\text{H}_2\text{O})_8]^{3+}$  ion will be discussed below. Furthermore, the hydration enthalpy of  $\text{Lu}^{3+}$  was simulated applying the DFT method and this procedure is presented in App. A.

### 3. Results

#### 3.1. The $[\text{Lu}(\text{OH}_2)_8]^{3+}$ (aq) Ion

$\text{Lu}^{3+}$  is strongly hydrated in aqueous solution as revealed by its large standard molar enthalpy of hydration ( $\Delta H_{\text{hyd}}^\theta$ ) at  $-3640 \text{ kJ}\cdot\text{mol}^{-1}$ . However, the  $\Delta H_{\text{hyd}}^\theta$ —values reported in the literature scatter from  $-3530$  to  $-3695 \text{ kJ}\cdot\text{mol}^{-1}$  [59–61]. Our DFT value for  $\Delta H_{\text{hyd}}^\theta$  at  $-3847.7 \text{ kJ}\cdot\text{mol}^{-1}$  is slightly smaller than the thermodynamic value (calculation procedure see Appendix A). The DFT optimized  $[\text{Lu}(\text{H}_2\text{O})_8]^{3+}$  geometry in the gas phase and also with a polarizable continuum (PC) model gave a square antiprismatic coordination polyhedron with symmetry  $S_8$  (Figure 1). Figure 1 shows both the hydrated ion and its  $\text{LuO}_8$  skeleton. Furthermore, the  $[\text{Lu}(\text{H}_2\text{O})_8]^{3+}$  aqua ion and its deuterated analog,  $[\text{Lu}(\text{D}_2\text{O})_8]^{3+}$ , imbedded in a PC were successfully simulated. The calculated Lu–O bond distance of the  $[\text{Lu}(\text{H}_2\text{O})_8]^{3+}$  ion with a solvation sphere (taking into account the influence of the bulk water) is in good agreement with the experimental value (Table 1). The discussion of the DFT frequencies of the cluster will be given below.

The vibrational analysis of the  $[\text{Lu}(\text{OH}_2)_8]^{3+}$  ( $S_8$  symmetry) with its 69 normal modes (n.m.s) leads to the irreducible representation:  $\Gamma_v(S_8) = 8a(\text{Ra}) + 9b(\text{i.r.}) + 18e_1(\text{Ra, i.r.}) + 18e_2(\text{n.a.}) + 16e_3(\text{n.a.})$  (Ra as Raman, i.r. as infrared and n.a. as not active). The modes with character a and  $e_1$  are Raman active and those with character b and  $e_3$  are i.r. allowed. The vibrations can be divided into 24 internal and 24 external vibrational modes of the coordinated water molecules plus 21 n.m.s of the  $\text{LuO}_8$  skeleton (a similar procedure has been given in ref. [62]).



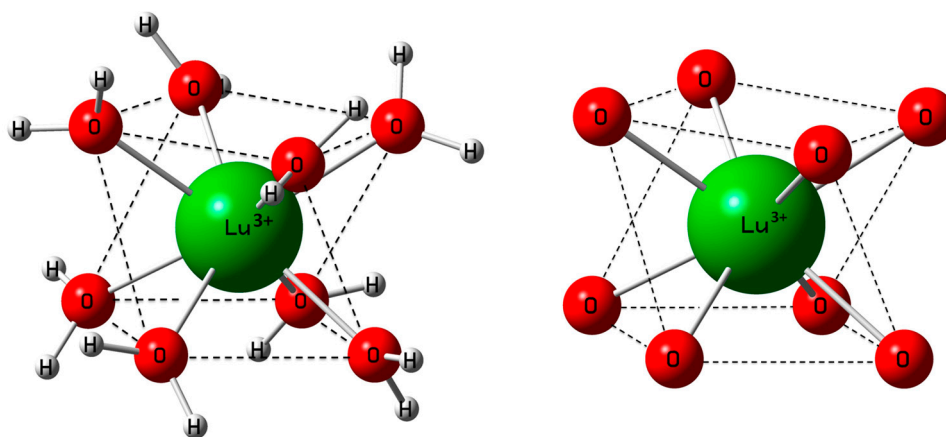


**Figure 1.** Left: Structure of the octaqua  $\text{Lu}^{3+}$ -ion (symmetry  $S_8$ ) as a gas phase cluster and imbedded in a polarizable dielectric continuum simulating the bulk water. At the right: The  $\text{LuO}_8$  skeleton ( $\text{H}_2\text{O}$  as point masses) with its  $D_{4d}$  symmetry.

**Table 1.** Geometrical parameters such as bond distances and angles of  $[\text{Lu}(\text{H}_2\text{O})_8]^{3+}$  imbedded in a polarizable dielectric continuum. Comparison of our DFT results (B3LYP/LANL2DZ) with published MD simulation and experimental results.

Bond Distances (Å) and Angels (°)	DFT Data/Gas Phase Cluster	DFT Data/Cluster + PC Model	ref. [25]	ref. [16]	ref. [24]	ref. [21]
Lu-O	2.350	2.311	2.338	2.307	2.37	2.32
O-H	0.981	0.982	-	-	-	-
H-O-H	109.29	110.45	-	-	-	-

The internal and external vibrations of the coordinated water may be considered separate from those of the  $\text{LuO}_8$  skeleton with the ligated water molecules seen as point masses. The  $\text{LuO}_8$  skeleton possesses  $D_{4d}$  symmetry and with its 9 atoms leads to 21 n.m.s and the irreducible representation is as follows:  $\Gamma_v(D_{4d}) = 2a_1(\text{Ra}) + b_1(\text{i.a.}) + 2b_2(\text{i.r.}) + 3e_1(\text{i.r.}) + 3e_2(\text{Ra}) + 2e_3(\text{Ra})$ . Although the  $\text{LuO}_8$  skeleton possesses no symmetry centre, the mutual exclusion rule is nevertheless effective. Seven modes with the character  $a_1$ ,  $e_2$  and  $e_3$  are Raman active while six modes with the character  $b_1$ ,  $b_2$  and  $e_1$  are i.r. allowed. The symmetric Lu-O stretch, the breathing mode, is only Raman active and appears strongly polarized in the Raman spectrum as the strongest band of the  $\text{LuO}_8$  skeleton spectrum. Two additional depolarized Raman active stretching modes are expected (character  $e_2$  and  $e_3$ ) as well as four other Raman deformation modes (character  $a_1$ ,  $e_2$  and  $e_3$ ). In I.R., two stretching modes (character  $b_2$  and  $e_1$ ) are expected and the remaining are deformations. In reality, however, the skeleton modes may not always be easily detected because they appear quite broad, weak and even obscured by the water background in solution.

Considering the coordinated water molecules of the  $[\text{Lu}(\text{OH}_2)_8]^{3+}$ -ion, the internal and external n.m.s of the water molecules may be divided into 24 internal and 24 external vibrations. These vibrations are derived from the rotational- and translational degrees of freedom of the isolated water molecule. The n.m.s of these water molecules, the external modes, are librational modes such as wag, twist, and rock [49,62]. In aqueous solutions, however, the librational modes are strongly overlapped with the librations of the bulk water and therefore not easily detected. They appear as weak, very broad modes below  $1200\text{ cm}^{-1}$  [62]. In addition to these librational modes, internal water modes are observed, the deformation mode,  $\nu_2(\text{H}_2\text{O})$  and two stretching OH modes,  $\nu_1$  and  $\nu_3$ . The deformation mode in liquid water is found at  $1640\text{ cm}^{-1}$  and the stretching modes at  $\sim 3400\text{ cm}^{-1}$  appear as a very broad structured band of H-bonded water molecules. The water modes are modified when coordinated to metal ions such as  $\text{Lu}^{3+}$  but are difficult to separate from the contributions of the librational and internal water modes of the bulk phase. In neat liquid water, the H-bonded water molecules show

broad and weak librational modes and internal water modes, the deformation band,  $\delta$  H-O-H, and the stretching O-H bands [29,62]. Spectra of liquid water and heavy water, bands and band assignments are given elsewhere [62].

The hydration sphere of  $\text{Lu}^{3+}$  (aq) is somewhat labile and a water-exchange rate constant  $k_{\text{ex}}$  at 25 °C was given at  $6 \times 10^7 \text{ s}^{-1}$  (from  $\text{H}_2\text{O}-\text{SO}_4^{2-}$  interchange rates [42,43]) with a water residence time  $\tau = 16.7 \text{ ns}$  and is slightly more labile than for instance  $[\text{Y}(\text{OH}_2)_8]^{3+}$  (aq) with  $\tau = 50 \text{ ns}$  [29]. On the other hand, it has a more rigid hydration sphere than  $[\text{La}(\text{OH}_2)_9]^{3+}$  with  $\tau = 5 \text{ ns}$  (aq). [27]. (The vibrational duration for the Lu-O breathing mode is 0.084 ps, short enough to allow  $\sim 199,000$  vibrations before the cluster experiences a water exchange. In other words, Raman spectroscopy probes an average hydration structure of rapidly exchanging water molecules in the direct vicinity of the  $\text{Lu}^{3+}$  ion.).

### 3.2. $\text{Lu}(\text{ClO}_4)_3$ and $\text{Lu}(\text{CF}_3\text{SO}_3)_3$ Solutions in Water and Heavy Water

$\text{Lu}(\text{ClO}_4)_3$  solution spectra: A Raman spectrum in the low frequency range of a  $0.186 \text{ mol}\cdot\text{L}^{-1}$   $\text{Lu}(\text{ClO}_4)_3$  solution (water to salt ratio at 289.0) is presented in Figure 2. Additionally, Raman spectra of two more concentrated  $\text{Lu}(\text{ClO}_4)_3$  solutions at  $2.233 \text{ mol}\cdot\text{L}^{-1}$  ( $R_w = 19.01$ ) and at  $0.556 \text{ mol}\cdot\text{L}^{-1}$  ( $R_w = 92.37$ ) are presented in Figures S1 and S2. The perchlorate ion has been chosen as a counterion because it is known as a weakly complex-forming ion. A high frequency band at  $3542 \text{ cm}^{-1}$  (fwhh =  $90 \text{ cm}^{-1}$ ), in the O-H stretching band region of  $\text{H}_2\text{O}$ , is observed in  $\text{Lu}(\text{ClO}_4)_3$  solutions which is attributed to an O-H band of weakly hydrated perchlorate ion (Figure S3 A/B). (In addition to the stretching mode  $\nu(\text{O}-\text{H}\cdots\text{ClO}_4^-)$  at  $3542 \text{ cm}^{-1}$  a very weak, broad mode appears in the terahertz region at  $\sim 165 \text{ cm}^{-1}$  in  $\text{Lu}(\text{ClO}_4)_3$  solutions ( $R_{\text{iso}}$ ). The latter mode has an equivalent in pure water at  $\sim 175 \text{ cm}^{-1}$  where it is moderately intense and slightly polarized. It is the restricted translational mode of the H-bonded water molecules ( $\text{O}\cdots\text{O}-\text{H}$ ). In concentrated  $\text{Lu}(\text{ClO}_4)_3$  solutions other H-bonds are important, namely  $\text{OH}\cdots\text{OClO}_3^-$  and the intensity of the band due to  $\text{HOH}\cdots\text{OClO}_3^-$  is extremely weak in the isotropic Raman spectrum [27–29]). For a detailed discussion on the influence of  $\text{ClO}_4^-$  on the stretching band on water in, for instance,  $\text{La}(\text{ClO}_4)_3$  (aq) and  $\text{Ce}(\text{ClO}_4)_3$  (aq) see [27,28].

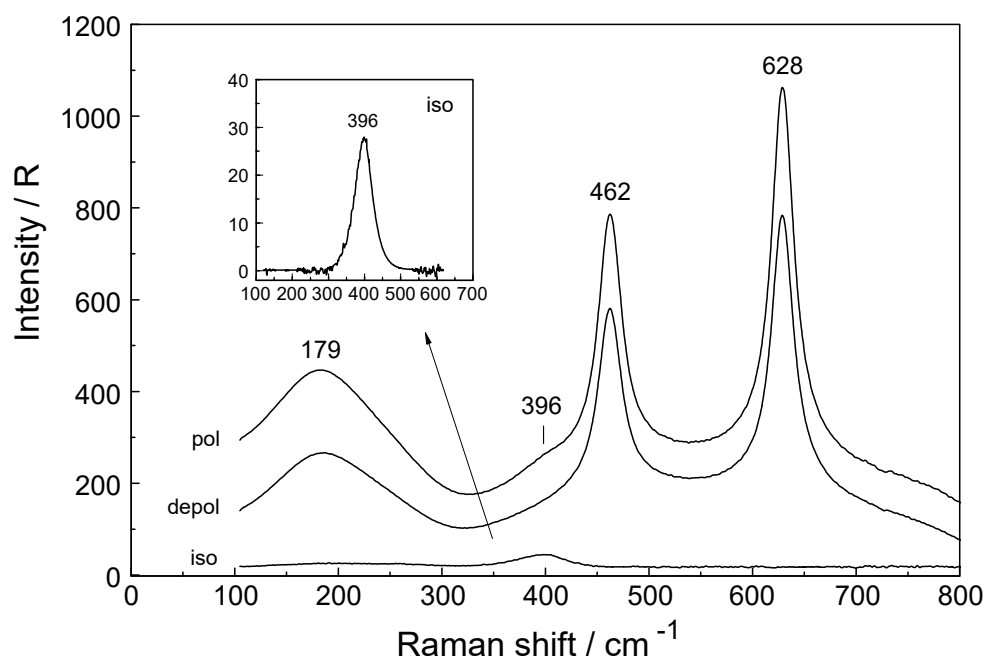


**Figure 2.** Raman spectrum in R-format (polarized, depolarized and isotropic scattering) of a  $0.186 \text{ mol}\cdot\text{L}^{-1}$   $\text{Lu}(\text{ClO}_4)_3$  solution ( $R_w = 289.0$ ). The isotropic band at  $396 \text{ cm}^{-1}$  is the symmetric stretching mode of the  $\text{LuO}_8$  skeleton of  $[\text{Lu}(\text{OH}_2)_8]^{3+}$ . The  $\text{ClO}_4^-$  (aq) deformation bands at  $462$  and  $628 \text{ cm}^{-1}$  are depolarized and do therefore not appear in the isotropic scattering. The broad band at  $179 \text{ cm}^{-1}$  is the restricted translation mode of water.

It is noteworthy to mention that the stretching band of  $\text{O-H}\cdots\text{OClO}_3^-$  is slightly cation dependent because of the different charge to radius ratios (polarizing power) of these ions. In  $\text{Lu}(\text{ClO}_4)_3$  (aq), the band appears at  $3542\text{ cm}^{-1}$ , slightly lower than in  $\text{La}(\text{ClO}_4)_3$  (aq) where it appears at  $3550\text{ cm}^{-1}$  [27].

The Raman spectrum of  $\text{ClO}_4^-$  (aq) ( $T_d$  symmetry) has been discussed in detail elsewhere so only a brief discussion shall be given [27–29]. The  $\text{ClO}_4^-$  ion possesses nine vibrational degrees of freedom and its internal vibrations span the representation  $\Gamma_{\text{vib}}(T_d) = a_1(\text{Ra}) + e(\text{Ra}) + 2f_2(\text{Ra, i.r.})$ . All four n.m.s are Raman active, but in i.r. only the  $f_2$  modes are allowed. In dilute solution, the symmetric Cl-O stretch,  $\nu_1(a_1)\text{ ClO}_4^-$  appears at  $931.5\text{ cm}^{-1}$  and is totally polarized ( $\rho = 0.005$ ) (fwhh =  $7.1\text{ cm}^{-1}$ ) and is the strongest mode in the Raman spectrum. The antisymmetric stretch,  $\nu_3(f_2)\text{ ClO}_4^-$  centred at  $1105\text{ cm}^{-1}$  and the deformation modes  $\nu_4(f_2)\text{ ClO}_4^-$  at  $629\text{ cm}^{-1}$  and  $\nu_2(e)\text{ ClO}_4^-$  at  $458\text{ cm}^{-1}$  are depolarized.

In a  $\text{Lu}(\text{ClO}_4)_3$  solution at  $0.186\text{ mol}\cdot\text{L}^{-1}$ , the  $\nu_1(a_1)\text{ ClO}_4^-$  band appears at  $931.8\text{ cm}^{-1}$  (fwhh =  $7.4\text{ cm}^{-1}$ ). In a concentrated solution ( $2.233\text{ mol}\cdot\text{L}^{-1}$ ) the  $\nu_1(a_1)\text{ ClO}_4^-$  band shifts to  $934.2\text{ cm}^{-1}$  and broadens (fwhh =  $12.0\text{ cm}^{-1}$ ). At the same time, the antisymmetric stretch,  $\nu_3(f_2)\text{ ClO}_4^-$  shifts to slightly higher wavenumbers and broadens.

The Raman spectra of  $\text{Lu}(\text{ClO}_4)_3$  (aq) reveal, in addition to the perchlorate-bands, weak bands in the low frequency region ( $50$  to  $400\text{ cm}^{-1}$ ) which are connected to  $\text{Lu}^{3+}$  (aq) species. In the isotropic scattering, a band appears at  $396\text{ cm}^{-1}$  which does not exist in  $\text{ClO}_4^-$  (aq). The band must stem from vibrations connected to the  $\text{LuO}_8$  skeleton. This isotropic band at  $396\text{ cm}^{-1}$  has a symmetrical profile with fwhh at  $50\text{ cm}^{-1}$ . In the totally symmetric stretching mode of the  $\text{LuO}_8$  skeleton, the  $\text{Lu}^{3+}$  ion remains stationary while the oxygen atoms vibrate without changing the symmetry of the  $\text{LuO}_8$  unit. (It is strongly polarized with a depolarization degree at 0.005). An example for the Raman spectrum of a  $0.186\text{ mol}\cdot\text{L}^{-1}$   $\text{Lu}(\text{ClO}_4)_3$  solution is given in Figure 2. In the anisotropic scattering, broad and very weak bands appear at  $113\text{ cm}^{-1}$ ,  $161.6\text{ cm}^{-1}$ ,  $231\text{ cm}^{-1}$ ,  $261.3\text{ cm}^{-1}$  and  $344\text{ cm}^{-1}$ . Figure 3 shows the weak anisotropic modes for a concentrated  $\text{Lu}(\text{ClO}_4)_3$  (aq) solution. Out of the seven theoretically predicted Raman modes only six could be observed. The second polarized  $\text{LuO}_8$  mode could not be observed. It is known that for hydrated metal ions in aqueous solution not all skeleton modes may be detected. In reality, the bands may be too broad and weak to be observed. The totally symmetric stretch, also called breathing mode of  $\text{LuO}_8$  is accompanied by a change in the polarizability ellipsoid but not in the dipole moment itself. This type of vibration which takes place with the conservation of all symmetry properties is thus called totally symmetric and has a depolarization degree  $\sim 0$ .

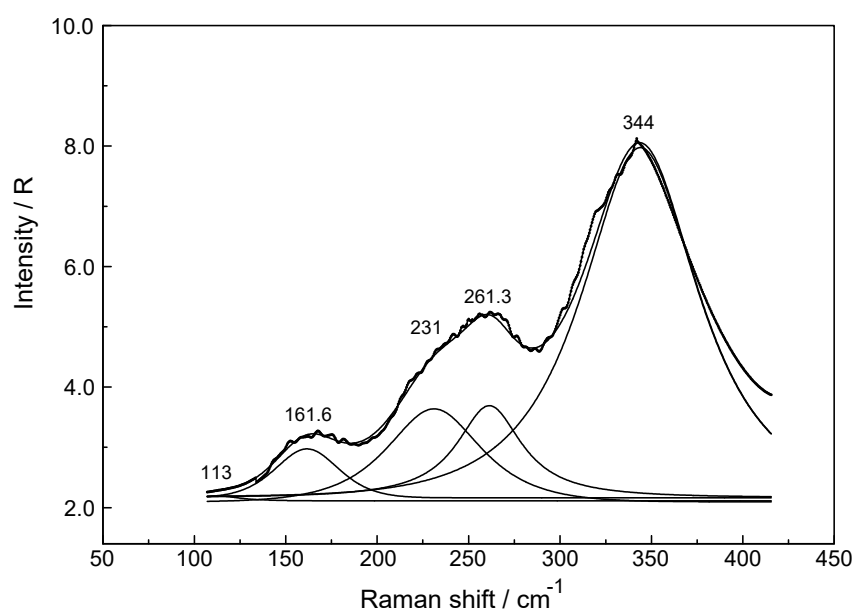


**Figure 3.** Anisotropic scattering profile in R-format of a  $2.233\text{ mol}\cdot\text{L}^{-1}$   $\text{Lu}(\text{ClO}_4)_3$  (aq) solution. Given are the measured curve, the sum curve and the 5 component bands of the band fit.



Replacing water with heavy water leads to an isotope shift to lower wavenumbers by a factor of  $\sim 0.948$  in  $\text{Lu}(\text{ClO}_4)_3(\text{D}_2\text{O})$ . The effect of deuteration on the  $\text{LuO}_8$  breathing mode was measured in  $\text{Lu}(\text{ClO}_4)_3\text{-D}_2\text{O}$  solutions and a band at  $376.5\text{ cm}^{-1}$  was observed (Figure S4). The theoretical shift of  $\nu_1$  on deuteration ( $\text{H}_2\text{O}/\text{D}_2\text{O}$  considered as point masses) is given according to:

$$\nu_1' = \nu_1[m(\text{H}_2\text{O})/m(\text{D}_2\text{O})]^{1/2} = (396\text{ cm}^{-1}) \times 0.948 = 375.6\text{ cm}^{-1} \quad (6)$$

(The simple formula for calculating the isotopic shift of the  $\nu_1$  mode is applicable because of the totally symmetric character of the normal mode of the  $\text{LuO}_8$  skeleton where  $\text{Lu}^{3+}$  remains stationary and only the oxygen atoms vibrate; the observed and theoretical depolarization degree is  $\sim 0$ .)

The agreement between the measured  $\nu_1$  symmetric stretch of the  $[\text{Lu}(\text{D}_2\text{O})_8]^{3+}$  species and the calculated one is excellent. Furthermore, the DFT result calculated for  $[\text{Lu}(\text{D}_2\text{O})_8]^{3+}$  with  $S_8$  symmetry imbedded in a PC leads to  $\nu_1 = 356.3\text{ cm}^{-1}$ . If the DFT value at  $376.3\text{ cm}^{-1}$  for  $[\text{Lu}(\text{H}_2\text{O})_8]^{3+}$  is used to calculate the breathing mode for  $[\text{Lu}(\text{D}_2\text{O})_8]^{3+}$ , according to Equation (5), a value at  $356.9\text{ cm}^{-1}$  follows. This agreement reinforces the assignment of this normal mode as a totally symmetric stretch with only insignificant contributions of the librations from heavy water.

Relative intensity measurements confirm that the scattering intensity of the  $\nu_1$  Lu-O mode is very weak with a scattering coefficient,  $S_h = 0.0024$ . The  $S_h$  values, defined as the R-corrected relative scattering efficiency of the M-O bands, were published for a variety of stretching modes of aqua metal ions in solution [27–29]. For  $\text{Y}^{3+}$ , for instance, which resembles properties of the heavy rare earths, its  $\nu_1$  breathing mode for  $[\text{Y}(\text{H}_2\text{O})_8]^{3+}$  appears at  $384\text{ cm}^{-1}$  [29] and also possesses a small relative intensity of 0.0025. Both ions,  $\text{Lu}^{3+}$  and  $\text{Y}^{3+}$ , have a low polarizability and are classified as hard cations according to Pearson's HSAB concept [63].

Perchlorate (Figure 2; Figures S1, S2 and S3A) was chosen as the counter ion because it is known as a weakly complex forming anion that does not substitute water in the first hydration sphere of the metal ions such as  $\text{Lu}^{3+}$ . However, in a  $\text{Lu}(\text{ClO}_4)_3$  (aq) at  $2.233\text{ mol}\cdot\text{L}^{-1}$ , the mole ratio solute to water is 19.01. This water content is barely enough to completely hydrate the  $\text{Lu}^{3+}$  ion while the remaining 11.1 water molecules hydrate the three  $\text{ClO}_4^-$  ions. In such a concentrated solution outer sphere ion pairs,  $[\text{Lu}(\text{OH}_2)_8]^{3+}\cdot\text{ClO}_4^-$  form and this explains the slight concentration dependence of the peak position appearing at  $394\text{ cm}^{-1}$  and the broadening of the band [27–29]. In a  $0.189\text{ mol}\cdot\text{L}^{-1}$   $\text{Lu}(\text{ClO}_4)_3$  solution, however, the  $\nu_1$   $\text{LuO}_8$  band occurs as a symmetrical band at  $396\text{ cm}^{-1}$  (fwhh at  $50\text{ cm}^{-1}$ ). A hydrolysis effect which might have been the cause of the changes of these bands can be ruled out in these acidic solutions. In a recent  $\text{La}(\text{ClO}_4)_3$  study on the influence of additional  $\text{HClO}_4$  in ternary solutions of  $\text{La}(\text{ClO}_4)_3$  plus  $\text{HClO}_4$ , measured in the low frequency region, the hydrolysis effect did not play a role at all [27–29].

To summarize: the Raman spectroscopy data clearly shows that in dilute  $\text{Lu}(\text{ClO}_4)_3$  (aq) an isotropic mode appears at  $396\text{ cm}^{-1}$  with fwhh =  $50\text{ cm}^{-1}$  which represents the breathing mode of the  $\text{LuO}_8$  skeleton. Furthermore, five additional weak and broad bands, depolarized in character, could be found in concentrated  $\text{Lu}(\text{ClO}_4)_3$  (aq).

DFT frequencies and assignments of the  $\text{LuO}_8$  modes: The DFT frequencies for the  $\text{LuO}_8$  skeleton modes for  $[\text{Lu}(\text{H}_2\text{O})_8]^{3+}$  imbedded in a polarizable dielectric continuum simulating the bulk water phase are given in Table S1. The totally symmetric stretch of the  $\text{LuO}_8$  skeleton  $\nu_1$   $\text{LuO}_8$  gave the wavenumber position at  $376.3\text{ cm}^{-1}$  in satisfactory agreement with the measured value (Table S1). The remaining 6 Raman active modes are in fair agreement with the measured ones considering the simple model used. One theoretical mode could not be detected. Table S1 presents and describes the theoretical  $\text{LuO}_8$  skeleton modes for  $[\text{Lu}(\text{H}_2\text{O})_8]^{3+}$  and its deuterated analog. Furthermore, the character of the  $\nu_1$   $\text{LuO}_8$  mode as a totally symmetric stretch with a depolarization degree zero was also verified. In contrast to the frequency in the condensed phase, the breathing mode for the  $[\text{Lu}(\text{OH}_2)_8]^{3+}$  in the gas phase gave a frequency value at  $347.1\text{ cm}^{-1}$ . The totally symmetric  $\text{LuO}_8$  stretch is called the breathing mode because while vibrating, the geometry of the cluster does not change its shape, the symmetry remains and therefore this mode is not allowed in i.r. The DFT frequency for  $\nu_1$   $\text{LuO}_8$  in

vacuo is much smaller than the one calculated with a polarizable continuum because the latter method takes into account the influence of the bulk water molecules. It is important to estimate the accuracy of the DFT method and such a brief discussion is given in Appendix B.

The hypothetical nonahydrate  $[\text{Lu}(\text{OH}_2)_9]^{3+}$  in vacuo with its tricapped trigonal prism (TTP) structure gave a much lower value for the symmetric stretching mode namely at  $329\text{ cm}^{-1}$  compared to  $347.1\text{ cm}^{-1}$  for the in vacuo frequency of  $[\text{Lu}(\text{OH}_2)_8]^{3+}$ . Furthermore, the Lu-O bond distances are much larger at  $2.448\text{ \AA}$  (three capping water molecules) and at  $2.379\text{ \AA}$  (6 prism water molecules). This is an additional and significant result for the existence of the octahydrate with its SAP structure.

To summarize, embedding the  $[\text{Lu}(\text{H}_2\text{O})_8]^{3+}$  species in a polarizable continuum, taking into account the effect of the bulk water, gave a reasonable agreement with the experimental frequencies found in  $\text{Lu}(\text{ClO}_4)_3$  (aq). Table S1 shows the results of all theoretical  $\text{LuO}_8$  modes for  $[\text{Lu}(\text{H}_2\text{O})_8]^{3+}$  and its deuterated analog. The DFT value for the Lu-O bond distance of the  $[\text{Lu}(\text{H}_2\text{O})_8]^{3+}$  at  $2.31\text{ \AA}$  is in good agreement with the experimental structural data (Table 1).

### 3.3. $\text{Lu}^{3+}$ -Trifluorosulfonate in Aqueous Solution

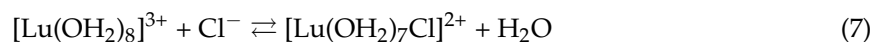
In  $\text{Lu}(\text{CF}_3\text{SO}_3)_3$  (aq), the Lu-O band is slightly overlapped with a polarized triflate band at  $319\text{ cm}^{-1}$  and appears at  $396.5\text{ cm}^{-1}$ . The Raman spectrum is shown in Figure S5. A band separation resulted in two bands with the first band component at  $319\text{ cm}^{-1}$  and the second band at  $396.5\text{ cm}^{-1}$  (fwhh =  $48\text{ cm}^{-1}$ ). The first band, a polarized band, stems from  $\text{CF}_3\text{SO}_3^-$  (aq) but the second, much weaker one, strongly polarized, represents the  $\text{LuO}_8$  breathing mode of  $[\text{Lu}(\text{H}_2\text{O})_8]^{3+}$ . The triflate in aqueous solution acts as a non-complexing anion and is suited, therefore, to study metal ion hydration. Band parameters and assignments of  $\text{CF}_3\text{SO}_3^-$  (aq) modes are given in ref. [29].

### 3.4. $\text{LuCl}_3$ (aq)

A Raman spectrum in R-format of two  $\text{LuCl}_3$  solutions, one at  $3.199\text{ mol}\cdot\text{L}^{-1}$  ( $R_w = 15.68$ ) and a more dilute one at  $0.478\text{ mol}\cdot\text{L}^{-1}$  ( $R_w = 166$ ) are presented in Figure 4A,B, respectively, in the wavenumber range from  $50\text{--}1300\text{ cm}^{-1}$ . The Lu-O stretching mode in the concentrated solution is down shifted and appears at  $390\text{ cm}^{-1}$  and an additional very broad isotropic component at  $205\text{ cm}^{-1}$  with a shoulder at  $\sim 254\text{ cm}^{-1}$  was observed. This finding is clear evidence that  $\text{Cl}^-$  substituted a water molecule in the first hydration shell of  $\text{Lu}^{3+}$ . The second isotropic band is due to the restricted translation mode of water and water/ $\text{Cl}^-$  at  $205\text{ cm}^{-1}$  (Figure 4A) while the broad band at  $254\text{ cm}^{-1}$  appearing as a shoulder has been assigned to a  $\text{Lu}(\text{OH}_2)_7^{3+}\text{Cl}^-$  stretching mode of a 1:1  $\text{Lu}^{3+}$ -chloro-complex,  $[\text{Lu}(\text{OH}_2)_7\text{Cl}]^{2+}$ . The concentration of the 1:1 chloro-complex species is in equilibrium with the fully hydrated species,  $[\text{Lu}(\text{OH}_2)_8]^{3+}$ . In contrast to concentrated  $\text{LuCl}_3$  solutions, the Lu-O stretching mode appears in dilute solutions ( $< 0.478\text{ mol}\cdot\text{L}^{-1}$ ) at  $396\text{ cm}^{-1}$  identical to the peak position in  $\text{Lu}(\text{ClO}_4)_3$  (aq). A dilution series presented in Figure 5 shows the shift of the Lu-O stretching mode to higher wavenumbers from  $390\text{ cm}^{-1}$  to  $396\text{ cm}^{-1}$ . In a  $3.199\text{ mol}\cdot\text{L}^{-1}$  solution with a mole ratio solute to water at 1 to 15.68, the peak appears at  $390\text{ cm}^{-1}$ , shifts to  $394\text{ cm}^{-1}$  for a solution at  $1.890\text{ mol}\cdot\text{L}^{-1}$  ( $R_w = 28.51$ ) and to  $395\text{ cm}^{-1}$  for a  $0.935\text{ mol}\cdot\text{L}^{-1}$  ( $R_w = 59.00$ ) solution and then remains constant at  $396\text{ cm}^{-1}$  for solutions  $< 0.478\text{ mol}\cdot\text{L}^{-1}$  ( $R_w = 115.99$ ). This frequency shift is accompanied by a change of the fwhh which becomes smaller with dilution and in solutions  $< 0.478\text{ mol}\cdot\text{L}^{-1}$  remains constant at  $50\text{ cm}^{-1}$ . This shows that with dilution the chloro-complex species disappears quickly and extrapolation of the Raman data show that in  $\text{LuCl}_3$  (aq)  $\leq 0.5\text{ mol}\cdot\text{L}^{-1}$  the  $\text{Lu}^{3+}$  cation is fully hydrated. Furthermore, the intensity of  $\nu_1\text{LuO}_8$  band as a function of concentration does not increase linearly in the  $\text{LuCl}_3$  solutions. However, the intensity increases less with concentration in contrast to the linear concentration dependence in  $\text{Lu}(\text{ClO}_4)_3$  (aq). Such a linear increase in band intensity would be expected if the octahydrated  $\text{Lu}^{3+}$  species remained the only stable species. This shows, clearly, that a chloro-complex species must have formed in higher concentrated solutions at the expense of the fully hydrated  $\text{Lu}^{3+}$ ,  $[\text{Lu}(\text{H}_2\text{O})_8]^{3+}$  ion (Figure 5). Quantitative Raman analysis revealed the species concentrations of fully hydrated  $\text{Lu}^{3+}$  (aq) and the

1:1 chloro-complex. The relationship between the integrated band intensity of  $\nu_1$  LuO<sub>8</sub>, I<sub>396</sub> and the solute concentration of Lu(ClO<sub>4</sub>)<sub>3</sub> is a linear one (see Equation (1); Experimental Sect.). The measured integrated band intensity of LuO<sub>8</sub> in LuCl<sub>3</sub> (aq), I<sub>396</sub>, follows the given linear relationship between I<sub>396</sub> and C<sub>T</sub> established in Lu(ClO<sub>4</sub>)<sub>3</sub> (aq) up to ~0.5 mol·L<sup>-1</sup> but then levels off noticeably at higher LuCl<sub>3</sub> concentrations (Figure S6). Obviously, above 0.5 mol·L<sup>-1</sup> LuCl<sub>3</sub> fractions of the fully hydrated Lu<sup>3+</sup> (aq) are converted to a 1:1 Lu<sup>3+</sup> chloro-complex species. The existence of higher chloro complexes than 1:1 can be convincingly ruled out taking into account the results of earlier anion exchange studies on aqueous rare earth chloride systems [37].

The mole fractions of both species are plotted in Figure 6. The fraction of the chloro-complex at 32%, in the most concentrated solution, is rather small and the fully hydrated species at 68% is still dominant. With dilution, the fraction of the chloro-complex species disappears quickly and at 0.5 mol·L<sup>-1</sup> it has vanished. It should be pointed out that the chloro-complex species is the only species detectable by Raman spectroscopy in agreement with the majority of the solution chemistry studies put forward [31–37]. The formation of the 1:1 chloro-complex may be formulated according to Equation (7):

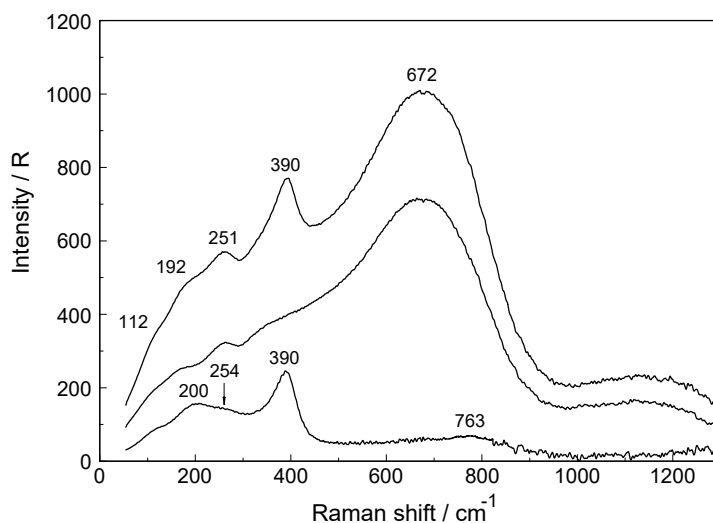


and the formation constant for the 1:1 Lu<sup>3+</sup>-chloro-complex formation, K<sub>1</sub>, is according to Equation (8):

$$K_1 = \frac{[\text{LuCl}^{2+}]}{[\text{Lu}^{3+}][\text{Cl}^-]} \times \frac{f_{\text{LuCl}_2^{2+}}}{f_{\text{Lu}^{3+}} \times f_{\text{Cl}^-}} \quad (8)$$

33 and with K<sub>1</sub>' the "concentration quotient" we get:

$$K_1 = K_1' \times \frac{f_{\text{LuCl}_2^{2+}}}{f_{\text{Lu}^{3+}} \times f_{\text{Cl}^-}}. \quad (9)$$



A

Figure 4. Cont.

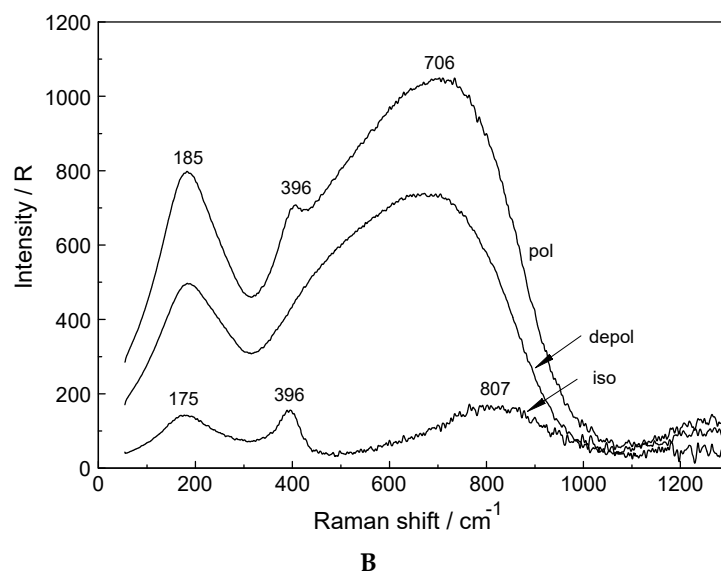


**Figure 4.** (A). Raman scattering profiles in R-format (from top to bottom: polarized, depolarized and isotropic scattering) of a  $3.199 \text{ mol}\cdot\text{L}^{-1}$   $\text{LuCl}_3$  solution. Note, the downshift of the Lu-O mode to  $390 \text{ cm}^{-1}$  compared to the one in  $\text{Lu}(\text{ClO}_4)_3$  (aq) (compare Figure 2) is due to the substitution of  $\text{Cl}^-$  for a water molecule in the first hydration sphere, forming  $[\text{Lu}(\text{OH}_2)_7\text{Cl}]^{2+}$ . The extremely broad mode at  $672 \text{ cm}^{-1}$  is due to the librational water band influenced by the solute. The mode at  $192 \text{ cm}^{-1}$  is due to the restricted O-H $\cdots$ O band of  $\text{H}_2\text{O}$  and the broad feature at  $\sim 251 \text{ cm}^{-1}$  is assigned to  $[\text{Lu}(\text{OH}_2)_7\text{Cl}]^{2+}$ . (B). Raman scattering profiles in R-format (from top to bottom: Polarized, depolarized and isotropic scattering) of a  $0.478 \text{ mol}\cdot\text{L}^{-1}$   $\text{LuCl}_3$  solution. Note, the  $\nu_1$  Lu-O mode at  $396 \text{ cm}^{-1}$  for  $[\text{Lu}(\text{OH}_2)_8]^{3+}$ . The extremely broad mode at  $807 \text{ cm}^{-1}$  in  $R_{\text{iso}}$  ( $R_{\text{pol}}$ :  $706 \text{ cm}^{-1}$ ) is due to the librational water band influenced by the solute. The mode at  $175 \text{ cm}^{-1}$  ( $R_{\text{iso}}$ ) is due to the restricted translation O-H $\cdots$ O band of  $\text{H}_2\text{O}$ .

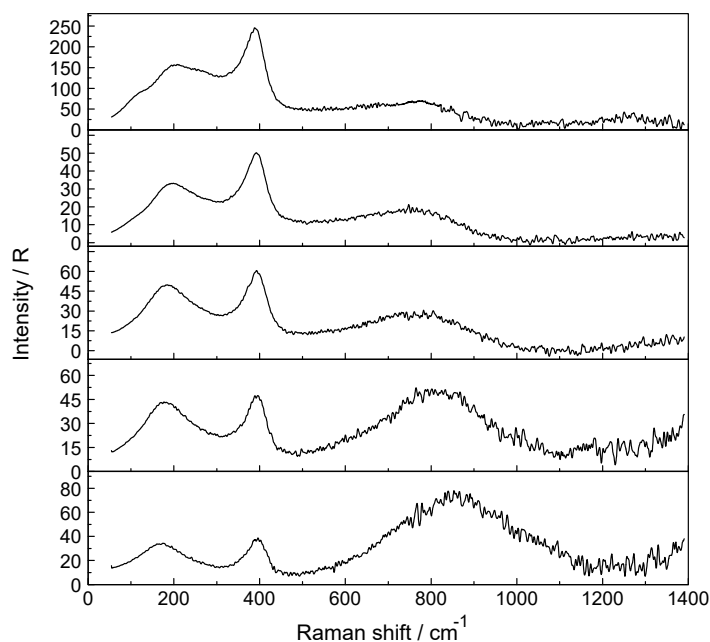


**Figure 5.** Isotropic Raman scattering profiles of aqueous  $\text{LuCl}_3$  solutions: from top to bottom:  $3.199 \text{ mol}\cdot\text{L}^{-1}$  ( $R_w = 15.68$ ),  $1.890 \text{ mol}\cdot\text{L}^{-1}$  ( $R_w = 28.51$ ),  $0.935 \text{ mol}\cdot\text{L}^{-1}$  ( $R_w = 98$ ),  $0.478 \text{ mol}\cdot\text{L}^{-1}$  ( $R_w = 116$ ) and  $0.241 \text{ mol}\cdot\text{L}^{-1}$  ( $R_w = 229.86$ ). The Lu-O mode in the most concentrated solution ( $3.199 \text{ mol}\cdot\text{L}^{-1}$ ) at  $390 \text{ cm}^{-1}$  compares to the one at  $396 \text{ cm}^{-1}$  in a  $0.241 \text{ mol}\cdot\text{L}^{-1}$   $\text{LuCl}_3$  (aq). This slight frequency shift is due to the substitution of  $\text{Cl}^-$  into the first hydration sphere, forming  $[\text{Lu}(\text{OH}_2)_7\text{Cl}]^{2+}$ . The broad feature at  $\sim 254 \text{ cm}^{-1}$  is assigned to  $[\text{Lu}(\text{OH}_2)_7\text{Cl}]^{2+}$ . See also Figure 4A,B.

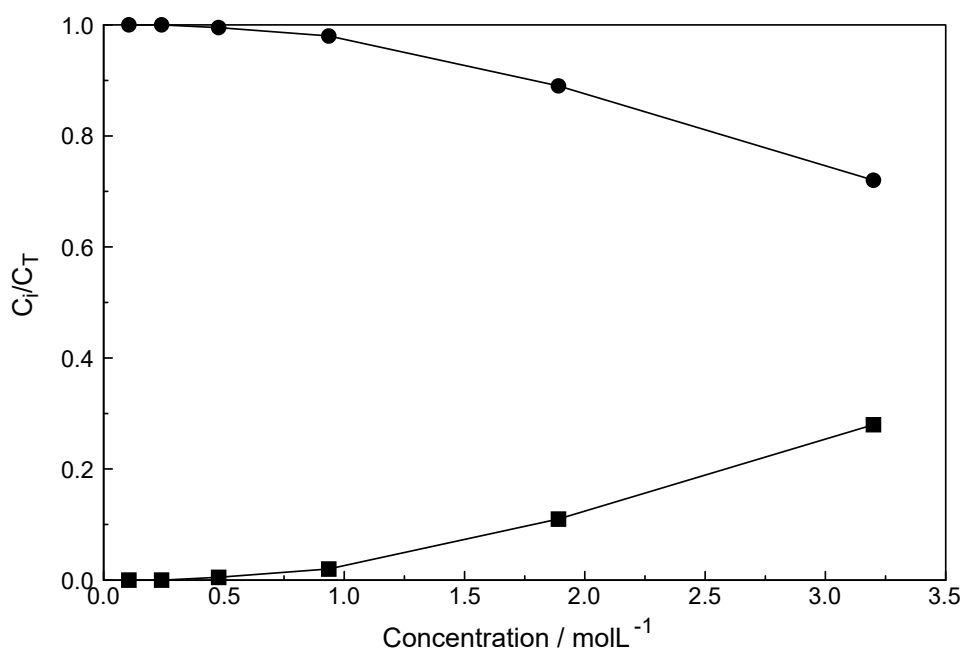


**Figure 6.** Fraction of species detected by quantitative Raman spectroscopy. The filled circles denote the  $[\text{Lu}(\text{OH}_2)_8]^{3+}$ , the fully hydrated  $\text{Lu}^{3+}$  and the filled squares the 1:1 chloro-complex species.

The concentration quotient can be measured by Raman spectroscopy according to Equation (10):

$$K_1' = \frac{(C_T - [\text{Lu}^{3+}])}{[\text{Lu}^{3+}] \times [\text{Cl}^-]} \quad (10)$$

where  $C_T$  is the total  $\text{LuCl}_3$  concentration and the concentrations in brackets denote the equilibrium concentrations of the fully hydrated  $\text{Lu}^{3+}$  and  $\text{Cl}^-$ . The equilibrium concentration of  $\text{Lu}^{3+}$  can be measured by Raman according to Equation (1) and thus we obtain  $K_1'$ .

The  $\log K_1'$  value measured by Raman spectroscopy is  $-0.62$  ( $I = 5.61 \text{ mol}\cdot\text{L}^{-1}$ ) and reveals the weak nature of the chloro-complex in  $\text{LuCl}_3$  (aq) at  $23^\circ\text{C}$ . Literature values for  $\log K_1$  for rare earth chlorides were compiled by Wood [31] and our  $\log K_1'$  fits reasonably well with the literature data given in ref. [31] Applying the specific ion interaction theory [64] in order to extrapolate  $\log K_1'$  to zero concentration, a  $\log K_1$  value at  $\sim -1.3$  is obtained. The nature of observed chloro-complex species has been controversially discussed. While NMR- and fluorescence spectroscopy [38–43] as well as the Raman effect detect chloro-complex species where chloride substitutes a water in the first hydration sphere, other methods such as ultrasound absorption [44–47] and DRS [30] may detect all 1:1 species, namely ion pairs where  $\text{Cl}^-$  is in the outer-sphere, in the outer-outer-sphere and also contact ion pairs/complex species. (DRS has however a considerable drawback in detecting complex species because symmetric complex species for which the dipole moment is zero cannot be probed.)

In a recent DRS study [30] the existence of outer-outer sphere ion pairs with two interposed water molecules was claimed to exist exclusively in  $\text{LaCl}_3$  solutions but no (direct ion pair) chloro-complex species could be detected. It is clear that different methods show different sensitivities probing species in aqueous solution. The sensitivity of DRS towards the different types of ion pairs is greatest for outer-outer sphere ion pairs less so for outer-sphere ion pairs and the least for complex species. Raman spectroscopy on the other hand fails to detect the outer-outer-sphere ion pairs but detects outer-sphere ion pairs and complex species/direct ion pairs. A Raman study taking into account the DRS data showed the different sensitivities for the detected species and this applies that different methods show different sensitivities toward the individual species [65]. For complete ion association models speciation data from different methods should be taken into account.



The weak chloro-complex species detected in  $\text{LuCl}_3$  (aq) could be also found in similar systems such as  $\text{LaCl}_3$  (aq),  $\text{CeCl}_3$  (aq) and  $\text{YCl}_3$  (aq) [27–29]. However, in  $\text{AlCl}_3$  solutions even at high concentrations,  $\text{Cl}^-$  does not substitute water of the first hydration shell of  $\text{Al}^{3+}$  [44,62] but forms outer-sphere ion pairs instead. The hydration shell of  $[\text{Al}(\text{OH}_2)_6]^{3+}$  is inert towards chloride substitution. Further experimental support for  $\text{Lu}^{3+}$ -chloride complex formation stems from a recent THz FTIR study on a similar system,  $\text{YbCl}_3$  (aq) and  $\text{YbBr}_3$  (aq). While in  $\text{YbCl}_3$  (aq) chloro-complex species albeit weak are formed no such species exist in the bromide system [66].

To further verify chloro-complex formation in  $\text{LuCl}_3$  (aq), HCl was added. A ternary  $\text{LuCl}_3$ -HCl solution composed of  $1.589 \text{ mol}\cdot\text{L}^{-1}$   $\text{LuCl}_3$  plus  $6.047 \text{ mol}\cdot\text{L}^{-1}$  HCl was measured and from its isotropic scattering profile the isotropic scattering contribution of a  $6.02 \text{ mol}\cdot\text{L}^{-1}$  HCl solution was subtracted. This difference spectrum reveals a band at  $386 \text{ cm}^{-1}$ , a prominent and broad, slightly asymmetric component at  $230 \text{ cm}^{-1}$  and a small scattering contribution at  $110 \text{ cm}^{-1}$  (Figure 7). Clearly, chloro-complex species are formed in these solutions and the common ion effect results in the formation of a second chloro-complex, a 1:2 complex species in addition to the 1:1 complex. Results of anion exchange experiments of metal ions in aqueous HCl solutions including  $\text{Lu}^{3+}$  showed that lutetium has a negligible adsorption [31,37]. Therefore, higher  $\text{Lu}^{3+}$ -chloro-complexes (complex anions) with  $n \geq 3$  can be ruled out. The formation of a second complex cation, the di-chloro-complex is formed according to Equation (11):

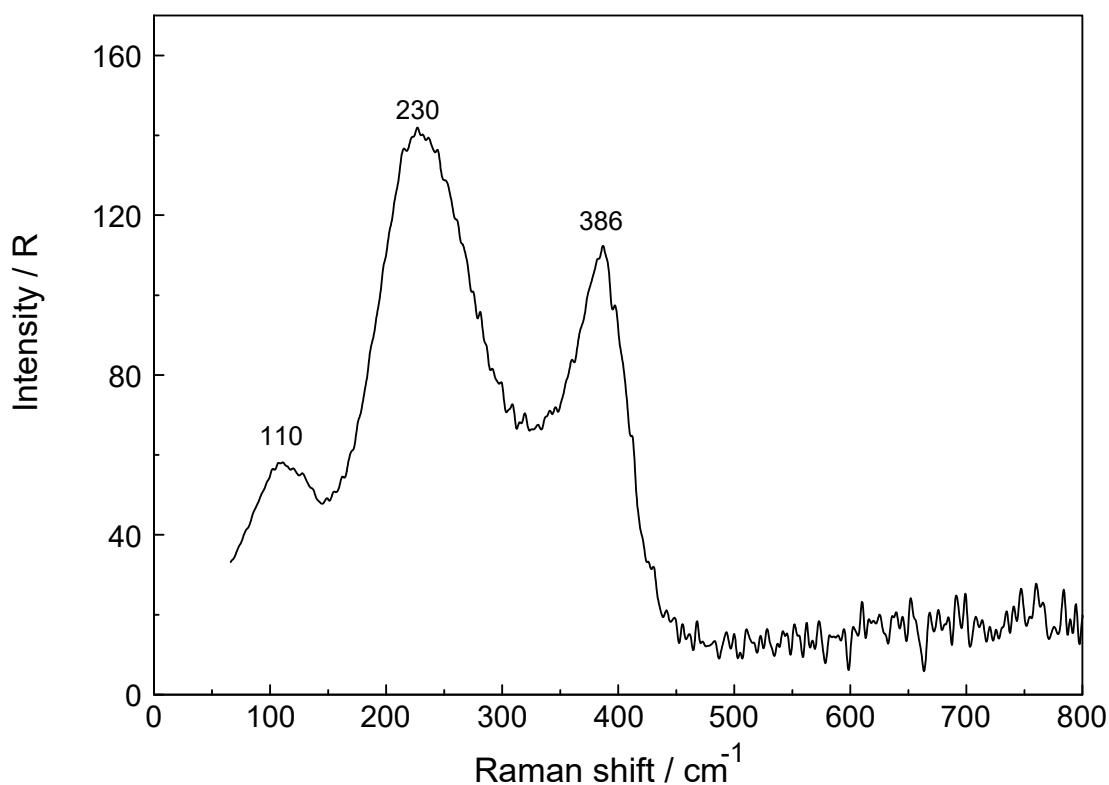
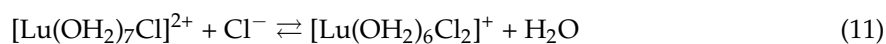


**Figure 7.** Isotropic Raman spectrum of a ternary  $\text{LuCl}_3$ /HCl composed of  $1.589 \text{ mol}\cdot\text{L}^{-1}$   $\text{LuCl}_3$  plus  $6.047 \text{ mol}\cdot\text{L}^{-1}$  HCl from which the isotropic scattering profile of a  $6.02 \text{ mol}\cdot\text{L}^{-1}$  HCl solution was subtracted. The difference spectrum shows clearly that  $\text{Cl}^-$  must have substituted water molecules of the first hydration sphere of  $\text{Lu}^{3+}$ . Lu-O mode of the complex,  $[\text{Lu}(\text{OH}_2)_{8-n}\text{Cl}_n]^{+3-n}$  ( $n = 1, 2$ ) and the broad mode at  $230 \text{ cm}^{-1}$  with a shoulder at  $263 \text{ cm}^{-1}$  and at  $110 \text{ cm}^{-1}$  are due to the chloro-complex species.

To summarize, a 1:1 chloro-complex species,  $[\text{Lu}(\text{OH}_2)_7\text{Cl}]^{2+}$  was detected in concentrated  $\text{LuCl}_3$  (aq) solution in equilibrium with the fully hydrated  $[\text{Lu}(\text{OH}_2)_8]^{3+}$  ion. The bands in the low frequency range assigned to the chloro-complex species could be characterized. A dilution series of  $\text{LuCl}_3$  solutions was studied by quantitative Raman spectroscopy and it could be shown that the chloro-complex dissociates completely to the  $[\text{Lu}(\text{OH}_2)_8]^{3+}$  (aq) and  $\text{Cl}^-$  (aq) ( $c < 0.5 \text{ mol}\cdot\text{L}^{-1}$ ). In other words the chloro-complex,  $[\text{Lu}(\text{OH}_2)_7\text{Cl}]^{2+}$ , is very weak and dissociates rapidly with dilution (increasing water activity).

#### 4. Conclusions

Raman spectra of aqueous  $\text{Lu}^{3+}$  perchlorate, triflate and chloride solutions were measured over a concentration range from  $0.105 \text{ mol}\cdot\text{L}^{-1}$  to  $3.199 \text{ mol}\cdot\text{L}^{-1}$ . The weak, isotropic mode at  $396 \text{ cm}^{-1}$  (fwhh =  $50 \text{ cm}^{-1}$ ) was assigned to  $\nu_1$  Lu-O of the  $\text{LuO}_8$  skeleton. In deuterated  $\text{Lu}(\text{ClO}_4)_3$  solutions, a mode at  $376 \text{ cm}^{-1}$  was assigned to the breathing mode,  $\nu_1$  Lu-O of  $[\text{Lu}(\text{OD}_2)_8]^{3+}$ . In the anisotropic scattering of aqueous  $\text{Lu}(\text{ClO}_4)_3$ , five bands of very low intensity were observed at  $113 \text{ cm}^{-1}$ ,  $161.6 \text{ cm}^{-1}$ ,  $231 \text{ cm}^{-1}$ ,  $261.3 \text{ cm}^{-1}$  and  $344 \text{ cm}^{-1}$ . Raman spectroscopic data suggest that perchlorate and triflate do not substitute water molecules in the first hydration sphere and the  $[\text{Lu}(\text{OH}_2)_8]^{3+}$  ion is stable in these solutions. Perchlorate and triflate are weakly complex forming anions. Although, no inner-sphere complex species could be detected in these solution, outer-sphere ion pairs of the type  $[\text{Lu}(\text{OH}_2)_8]^{3+}\cdot\text{ClO}_4^-$  may be formed in concentrated  $\text{Lu}(\text{ClO}_4)_3$  (aq). DFT frequency calculations of a  $[\text{Lu}(\text{OH}_2)_8]^{3+}$  imbedded in a polarizable dielectric continuum gave a  $\nu_1$  Lu-O equal to  $376.3 \text{ cm}^{-1}$  in fair agreement with the experiment. The bond distances and angles of the  $[\text{Lu}(\text{OH}_2)_8]^{3+}$  imbedded in a polarizable dielectric continuum were also presented. The hydration enthalpy for  $\text{Lu}^{3+}$  (aq) could be simulated by DFT and  $\Delta H_{\text{hyd(l)}} = -3847.7 \text{ kJ/mol}$  was obtained in fair agreement with experimental values.

In  $\text{LuCl}_3$  solutions, in addition to the breathing mode,  $\nu_1$  Lu-O of  $[\text{Lu}(\text{OH}_2)_8]^{3+}$ , a second isotropic mode at  $254 \text{ cm}^{-1}$  was verified. This new mode has been assigned to a  $\text{Lu}^{3+}$ -chloro-complex species. A chloride ion, thereby, substitutes a water molecule of the first hydration sphere of  $\text{Lu}^{3+}$  (aq) forming a 1:1 chloro-complex. This is proof of the lability of the first hydration sphere of  $\text{Lu}^{3+}$  (aq). The Raman spectroscopic characterization of a 1:1 chloro-complex confirms recent results applying neutron- and X-ray scattering as well as EXAFS [12,20]. Quantitative Raman measurements allowed the determination of the fraction of the 1:1 chloro-complex and the fully hydrated species in concentrated  $\text{LuCl}_3$  solutions down to  $\sim 0.5 \text{ mol}\cdot\text{L}^{-1}$  where the chloro-complex vanishes.

**Supplementary Materials:** The following are available online. Figure S1: Raman scattering profiles in R-format (from top to bottom: polarized, depolarized and isotropic scattering profiles) of a  $2.233 \text{ mol}\cdot\text{L}^{-1}$   $\text{Lu}(\text{ClO}_4)_3$  solution ( $R_w = 19.01$ ). The  $\text{ClO}_4^-$  (aq) deformation bands at  $462$  and  $628 \text{ cm}^{-1}$  are depolarized and therefore do not appear in the isotropic scattering. The inset shows  $\nu_1$  Lu-O stretching mode at  $394 \text{ cm}^{-1}$ , the breathing mode of the  $\text{LuO}_8$  skeleton at the terahertz frequency range. The isotropic scattering profile is given. Figure S2: Raman scattering profiles in R-format (polarized, depolarized and isotropic scattering profiles) of a  $0.556 \text{ mol}\cdot\text{L}^{-1}$   $\text{Lu}(\text{ClO}_4)_3$  solution ( $R_w = 92.37$ ). The  $\text{ClO}_4^-$  (aq) deformation bands at  $462$  and  $628 \text{ cm}^{-1}$  are depolarized and therefore do not appear in the isotropic scattering. The inset shows symmetric stretching mode,  $\nu_1$  Lu-O, called the breathing mode of the  $\text{LuO}_8$  skeleton at the terahertz frequency range at a larger scale. All scattering profiles are given. Figure S3A: Overview Raman scattering profiles in R-format (from top to bottom: polarized, depolarized and isotropic scattering profiles) of a  $2.233 \text{ mol}\cdot\text{L}^{-1}$   $\text{Lu}(\text{ClO}_4)_3$  solution ( $R_w = 19.01$ ) from  $50$ – $1400 \text{ cm}^{-1}$ . The  $\text{ClO}_4^-$  (aq) deformation bands at  $462$  and  $628 \text{ cm}^{-1}$  are depolarized and therefore do not appear in the isotropic scattering. The symmetric stretching mode,  $\nu_1$  of  $\text{ClO}_4^-$  (aq) appears at  $934 \text{ cm}^{-1}$  and the antisymmetric stretching mode  $\nu_3$  of  $\text{ClO}_4^-$  (aq) appears as a depolarized mode at  $1112 \text{ cm}^{-1}$ . The inset at the left side shows  $\nu_1$  Lu-O stretching mode at  $394 \text{ cm}^{-1}$  the breathing mode of the  $\text{LuO}_8$  skeleton at the terahertz frequency range at a larger scale. The inset at the right side shows the  $\nu_1$   $\text{ClO}_4^-$  band at  $934 \text{ cm}^{-1}$  at its full scale. Figure S3B: Raman profiles of the same  $2.233 \text{ mol}\cdot\text{L}^{-1}$   $\text{Lu}(\text{ClO}_4)_3$  solution in the wavenumber region from  $1400 \text{ cm}^{-1}$  to  $4160 \text{ cm}^{-1}$  (from top to bottom: Polarized, depolarized and isotropic scattering profiles). The deformation mode of water appears at  $1623 \text{ cm}^{-1}$  and in the O-H stretching region the water band is modified by the typical  $\text{ClO}_4^- \cdots \text{H}_2\text{O}$  mode of weakly hydrogen bonded O-H oscillators. The strong prominent band at  $3542 \text{ cm}^{-1}$  is due to the weakly bonded O-H $\cdots$ O units of water  $\cdots\text{ClO}_4^-$ . Figure S4: Raman spectrum in R-format (from top to bottom: Polarized,

depolarized and isotropic scattering profiles) of a 0.439 mol·L<sup>-1</sup> Lu(ClO<sub>4</sub>)<sub>3</sub> solution in D<sub>2</sub>O. The ClO<sub>4</sub><sup>-</sup> (D<sub>2</sub>O) deformation bands at 462 and 629 cm<sup>-1</sup> are depolarized and therefore do not appear in the isotropic scattering. The symmetric stretching mode, ν<sub>1</sub> ClO<sub>4</sub><sup>-</sup> (D<sub>2</sub>O) appears at 933 cm<sup>-1</sup> and the antisymmetric stretching mode, ν<sub>3</sub> ClO<sub>4</sub><sup>-</sup> (D<sub>2</sub>O) at 1108 cm<sup>-1</sup>. The latter mode is depolarized. The Lu-O breathing mode is shifted to 376.5 cm<sup>-1</sup> compared to the mode in Lu(ClO<sub>4</sub>)<sub>3</sub> in H<sub>2</sub>O, where it appears at 396 cm<sup>-1</sup>. The band marked with the symbol (+) at 1202 cm<sup>-1</sup>, partially polarized, is due to the deformation mode of D<sub>2</sub>O. Figure S5: Isotropic Raman scattering profile (R-format) of a 1.05 mol·L<sup>-1</sup> Lu(CF<sub>3</sub>SO<sub>3</sub>)<sub>3</sub> solution. Next to the strong band of triflate at 319.5 cm<sup>-1</sup> appears a small and relatively broad band at 396.5 cm<sup>-1</sup> which is due to the totally symmetric stretching mode of LuO<sub>8</sub>. Figure S6: Linear regression line of the integrated band intensity I<sub>396</sub> as a function of the Lu(ClO<sub>4</sub>)<sub>3</sub> solution concentration (black circles); upper curve depicts: I<sub>396</sub> = 1148.3 × C<sub>T</sub>, the calibration curve. The lower curve shows the integrated band intensities in LuCl<sub>3</sub> solutions (black squares). Table S1: Assignment and approximate description of the calculated vibrational modes using B3LYP/SDD of [Lu(H<sub>2</sub>O)<sub>8</sub>]<sup>3+</sup> and [Lu(D<sub>2</sub>O)<sub>8</sub>]<sup>3+</sup> applying the PC model to the contribution of the normal modes of the LuO<sub>8</sub> skeleton.

**Author Contributions:** Conceptualization, W.R.; Methodology, W.R.; Software, G.I.; Validation, W.R. and G.I.; Formal Analysis, W.R. and G.I.; Investigation, W.R. and G.I.; Resources, W.R. and G.I.; Data Curation, W.R.; Writing-Original Draft Preparation, W.R.; Writing-Review & Editing, W.R.; Visualization, W.R. and G.I.; Supervision, Project Administration, W.R.

**Funding:** This research received no external funding.

**Acknowledgments:** We thank J. Kortus of the Institut für Theoretische Physik, TU Bergakademie Freiberg, Germany for his hospitality and permission for the use of the Raman spectrometer. We are grateful to the colleagues of the Institut for their hospitality and stimulating discussions. We particularly wish to acknowledge Frau B. Ostermayr for her help in measuring the samples.

**Conflicts of Interest:** The authors declare no conflict of interest.

## Appendix A

### Hydration Enthalpy: Comparison of Calculated Values with Experimental Ones

Comparison of the binding energies obtained by DFT calculations at T = 0 K with thermochemical measurements of the hydration enthalpy carried out with vibrating molecules usually at 298 K requires corrections for the translational, rotational and vibrational energy. For one mole molecules of an ideal gas, one obtains the enthalpy:

$$H(T) = E_e + E_t(T) + E_r(T) + E_v(T) + RT \quad (12)$$

Here, E<sub>e</sub> stands for the electronic energy, E<sub>t</sub>(T) the translational energy, E<sub>r</sub>(T) the rotational energy, and E<sub>v</sub>(T) = N<sub>h</sub> ∑<sub>i</sub> ν<sub>i</sub> (1/2 + 1/(e<sup>hν<sub>i</sub>/kT</sup> - 1)) is the thermal vibrational energy. The calculation of the hydration enthalpy in the liquid state, ΔH<sub>hyd(l)</sub> for [Lu(OH<sub>2</sub>)<sub>8</sub>]<sup>3+</sup> requires consideration of additional contributions. According to a Born-Haber cycle it follows:

$$\Delta H_{\text{hyd(l)}} \approx \Delta H_{\text{cluster}} + \Delta H_{\text{solv}} + \Delta H_{\text{vap}} \\ \text{with } \Delta H_{\text{cluster}} = H[\text{Lu}(\text{OH}_2)_8]^{3+} - H(\text{Lu}^{3+}) - 8 \times H(\text{OH}_2) \quad (13)$$

Here, ΔH<sub>cluster</sub> is the cluster binding enthalpy, ΔH<sub>solv</sub> means the solvation enthalpy resulting from the transfer of the gas phase cluster to the liquid state. The solvation enthalpy ΔH<sub>solv</sub> can be estimated with the PC model by placing the [Lu(OH<sub>2</sub>)<sub>8</sub>]<sup>3+</sup> cluster in a polarizable dielectric and so taking into account the bulk water and comparing the polarized solute with the solvent. ΔH<sub>vap</sub> is the heat of water vaporization of the 8 water molecules. With ΔH<sub>cluster</sub> = -2671.6 kJ/mol, ΔH<sub>solv</sub> = -1528.2 kJ/mol, and ΔH<sub>vap</sub> = 352.2 kJ/mol we obtain for the hydration enthalpy ΔH<sub>hyd(l)</sub> = -3847.7 kJ/mol. Experimental values for the standard molar hydration enthalpy ΔH<sub>hyd(l)</sub>(298) of Lu<sup>3+</sup> in the liquid state are: -3530 kJ/mol [59] and -3695 kJ/mol [60]. The correspondence with the theoretical values is satisfactory in consideration of the simple set of basis functions that has been used and the simplifications of the PC model which uses the constant dielectric constant of bulk water (ε = 81) outside of the cluster. However, due to orientation polarization in the cation field, the orientation of

the water molecule dipoles change in a transition region outside the first hydration shell from strongly oriented to orientation at random in the bulk water. This comes along with a gradual rise of the dielectric constant up to the bulk value. Following Debye [67], the transition range for different cations can be calculated to be between 10 Å and 20 Å and the absolute value of the hydration enthalpy is diminished between 1% and 5% in comparison with the case of  $\epsilon = 81$  assumption. For  $\text{Lu}^{3+}$  hydration, values of about 13 Å and 3% can be estimated for this model.

## Appendix B

### Accuracy of the DFT Method

The B3LYP method used seems to be suitable to describe properties of the  $[\text{Lu}(\text{OH}_2)_8]^{3+}$  cluster reliably. For the cluster  $[\text{Lu}(\text{OH}_2)_8]^{3+}$  in vacuo the totally symmetric stretching mode  $\nu_1\text{LuO}_8$  at  $347.1\text{ cm}^{-1}$  and the Lu-O bond distance at  $2.350\text{ Å}$  was obtained. Ab initio methods such as MP2 give similar results  $\nu_1\text{LuO}_8$  at  $356.5\text{ cm}^{-1}$  and the Lu-O bond distance at  $2.305\text{ Å}$  but 20 times more time consuming. The HF method results in  $\nu_1\text{LuO}_8$  at  $347.1\text{ cm}^{-1}$  and the Lu-O bond distance at  $2.376\text{ Å}$ . In all these cases the SDD basis set was used. Also, other basis sets and density functional dependence of  $\text{Ln}^{3+}$ -hydrates were systematically investigated recently; again for clusters in vacuo [68].

However, applying B3LYP/SDD and using the polarizable continuum model the deviation between the calculated and the experimentally observed for the totally symmetric stretching mode  $\nu_1\text{LuO}_8$  and the Lu-O bond distance amounts to 5% and 2%, respectively. This dictates that the inclusion of the bulk water beyond the first hydration sphere is necessary to obtain realistic cluster frequencies in solution. (Some shortcomings of the PCM model are mentioned in Appendix A).

## References

1. Taylor, S.; McClennan, S. *The Continental Crust: Its Composition and Evolution*; Blackwell Scientific Publications: Oxford, UK, 1985.
2. Cotton, S. *Lanthanide and Actinide Chemistry*; John Wiley & Sons: Chichester, West Sussex, UK, 2006.
3. Emsley, J. *Nature's Building Blocks: An A-Z Guide to the Elements, Lutetium*; Oxford University Press: Oxford, UK, 2011; pp. 240–242.
4. Huang, C.-H.; Bian, Z. *Introduction in Rare Earth Coordination Chemistry: Fundamentals and Applications*; Huang, C.-H., Ed.; John Wiley & Sons Wiley: Chichester, West Sussex, UK, 2010.
5. Zimmerman, P.A.; Rice, B.J.; Piskanib, E.C.; Liberman, V. *Optical Microlithography XXII*; Levinson, H.J., Dusa, M.V., Eds.; Proc. of SPIE: Bellingham, WA, USA, 2009; Volume 7274-11, p. 727420.
6. Yao, R.; Ma, T.; Shao, Y. Lutetium oxyorthosilicate (LSO) intrinsic activity correction and minimal detectable target activity study for SPECT imaging with a LSO-based animal PET scanner. *Phys. Med. Biol.* **2008**, *53*, 4399. [[CrossRef](#)] [[PubMed](#)]
7. Lapen, T.J.; Righter, M.; Brandon, A.D.; Debaille, V.; Beard, B.L.; Shafer, J.T.; Peslier, A.H. A Younger Age for ALH84001 and Its Geochemical Link to Shergottite Sources in Mars. *Science* **2010**, *328*, S347–S351. [[CrossRef](#)] [[PubMed](#)]
8. Ferreira, K.M.; Collins, S.M.; Fenwick, A.J. International Conference on Nuclear Data for Science and Technology. In Proceedings of the EPJ Web of Conferences, Bruges, Belgium, 11–16 September 2016; ND 2016, p. 08002-5.
9. U.S. Food & Drug Administration. January 2018. Available online: <https://www.fda.gov/Drugs/.../ApprovedDrugs/ucm594105.htm>. (accessed on 26 January 2018).
10. Krishnamurthy, N.; Gupta, C.K. *Extractive Metallurgy of Rare Earths*, 2nd ed.; CRC Press: Boca Raton, FL, USA, 2015.
11. Brown, P.L.; Ekberg, C. *Hydrolysis of Metal Ions*, 1st ed.; Wiley-VCH: Weinheim, Germany, 2016.
12. Spedding, F.H.; Pikal, M.; Ayers, B. Apparent Molal Volumes of Some Aqueous Rare Earth Chloride and Nitrate Solutions at  $25^\circ$ . *J. Phys. Chem.* **1966**, *70*, 2440–2449. [[CrossRef](#)]

13. Spedding, F.H.; Shiers, L.E.; Brown, M.A.; Derer, J.L.; Swanson, D.L.; Habenschuss, A.J. Densities and apparent molal volumes of some aqueous rare earth solutions at 25.deg. II. Rare earth perchlorates. *J. Chem. Eng. Data* **1975**, *20*, 81–88. [[CrossRef](#)]
14. Spedding, F.H.; Cullen, P.F.; Habenschuss, A. Apparent molal volumes of some dilute aqueous rare earth salt solutions at 25.deg. *J. Phys. Chem.* **1974**, *78*, 1106–1110. [[CrossRef](#)]
15. Cossy, C.; Merbach, A.E. Recent Developments in Solvation and Dynamics of the Lanthanide (III) Ions. *Pure Appl. Chem.* **1988**, *60*, 1785–1796. [[CrossRef](#)]
16. Persson, I.; D'Angelo, P.; Panifilis, S.D.; Sandström, M.; Eriksson, L. Hydration of Lanthanoid(III) Ions in Aqueous Solution and Crystalline Hydrates Studied by EXAFS Spectroscopy and Crystallography: The Myth of the “Gadolinium Break”. *Chem.-Eur. J.* **2008**, *14*, 3056–3066. [[CrossRef](#)]
17. D'Angelo, P.; Spezia, R. Hydration of Lanthanoids(III) and Actinoids(III): An Experimental/Theoretical Saga. *Chem.-Eur. J.* **2012**, *18*, 11162–11178. [[CrossRef](#)] [[PubMed](#)]
18. Duvail, M.; D'Angelo, P.; Gageot, M.-P.; Vitorge, P.; Spezia, R. What first principles molecular dynamics can tell us about EXAFS spectroscopy of radioactive heavy metal cations in water. *Radiochim. Acta* **2009**, *97*, 339–346. [[CrossRef](#)]
19. Zhang, J.; Heinz, N.; Dolg, M. Understanding Lanthanoid(III) Hydration Structure and Kinetics by Insights from Energies and Wave functions. *Inorg. Chem.* **2014**, *53*, 7700–7708. [[CrossRef](#)] [[PubMed](#)]
20. Hitzengerger, M.; Hofer, T.; Weiss, A. Solvation properties and behaviour of lutetium(III) in aqueous solution—A quantum mechanical charge field (QMCF) study. *J. Chem. Phys.* **2013**, *139*, 114306-7. [[CrossRef](#)] [[PubMed](#)]
21. Sessa, F.; Spezia, R.; D'Angelo, P. Lutetium(III) aqua ion: On the dynamical structure of the heaviest lanthanoid hydration complex. *J. Chem. Phys.* **2016**, *144*, 204505. [[CrossRef](#)] [[PubMed](#)]
22. Ishiguro, S.-I.; Umebayashi, Y.; Kato, K.; Takahashib, R.; Ozutsumi, K. Strong and weak solvation steric effects on lanthanoid(III) ions in *N,N*-dimethylformamide-*N,N*-dimethylacetamide mixtures. *J. Chem. Soc., Faraday Trans.* **1998**, *94*, 3607–3612. [[CrossRef](#)]
23. Yaita, T.; Narita, H.; Suzuki, S.; Tachimori, S.; Motohashi, H.; Shiwaku, H. Structural study of lanthanides(III) in aqueous nitrate and chloride solutions by EXAFS. *J. Radioanal. Nucl. Chem.* **1999**, *239*, 371–375. [[CrossRef](#)]
24. Rogers, R.D.; Kurihara, L.K. f-element/crown ether complexes. 6. Interaction of hydrated lanthanide chlorides with 15-crown-5: Crystallization and structures of  $[M(OH_2)_8]Cl_3 \cdot (15\text{-crown-5})$  ( $M = Gd, Lu$ ). *Inorg. Chim. Acta* **1987**, *130*, 131–137. [[CrossRef](#)]
25. Habenschuss, A.; Spedding, F.H. The coordination (hydration) of rare earth ions in aqueous chloride solutions from x ray diffraction. I.  $TbCl_3$ ,  $DyCl_3$ ,  $ErCl_3$ ,  $TmCl_3$ , and  $LuCl_3$ . *J. Chem. Phys.* **1979**, *70*, 2797–2806. [[CrossRef](#)]
26. Migliorati, V.; Serva, A.; Sessa, F.; Lapi, A.; D'Angelo, P. Influence of Counterions on the Hydration Structure of Lanthanide Ions in Dilute Aqueous Solutions. *J. Phys. Chem. B* **2018**, *122*, 2779–2791. [[CrossRef](#)]
27. Rudolph, W.W.; Irmer, G. Hydration and ion pair formation in common aqueous La(III) salt solutions—a Raman scattering and DFT study. *Dalton Trans.* **2015**, *44*, 295–305. [[CrossRef](#)]
28. Rudolph, W.W.; Irmer, G. Raman spectroscopic characterization of light rare earth ions:  $La^{3+}$ ,  $Ce^{3+}$ ,  $Pr^{3+}$ ,  $Nd^{3+}$  and  $Sm^{3+}$  – hydration and ion pair formation. *Dalton Trans.* **2017**, *46*, 4235–4244. [[CrossRef](#)]
29. Rudolph, W.W.; Irmer, G. Hydration and ion pair formation in aqueous  $Y^{3+}$ -salt solutions. *Dalton Trans.* **2015**, *44*, 18492–18505. [[CrossRef](#)]
30. Friesen, S.; Krickl, S.; Luger, M.; Nazet, A.; Hefter, G.; Buchner, R. Hydration and ion association of  $La^{3+}$  and  $Eu^{3+}$  salts in aqueous solution. *Phys. Chem. Chem. Phys.* **2018**, *20*, 8812–8821. [[CrossRef](#)] [[PubMed](#)]
31. Wood, S.A. The aqueous geochemistry of the rare-earth elements and yttrium. 1. Review of available low-temperature data for inorganic complexes and the inorganic REE speciation of natural waters. *Chem. Geol.* **1990**, *82*, 159–186. [[CrossRef](#)]
32. Peppard, D.F.; Mason, G.W.; Hucher, I. Stability constants of certain lanthanide(III) and actinide(III) chloride and nitrate complexes. *J. Inorg. Nucl. Chem.* **1962**, *24*, 881–888. [[CrossRef](#)]
33. Sekine, T. Complex formation of Lu(III), Eu(III), Lu(III) and Am(III) with oxalate, sulphate, chloride and thiocyanate ions. *J. Inorg. Nucl. Chem.* **1964**, *26*, 1463–1465. [[CrossRef](#)]
34. Fukasawa, T.; Kawasuji, I.; Mitsugahiro, T.; Sat, A.; Suzuki, S. Investigation on the Complex Formation of Some Lanthanoids(III) and Actinoids(III) with chloride and Bromide. *Bull. Chem. Soc. Japan* **1982**, *55*, 726–729. [[CrossRef](#)]



35. Choppin, G.R.; Unrein, P.J. Halide complexes of the lanthanide elements. *J. Inorg. Nucl. Chem.* **1963**, *25*, 387–393. [[CrossRef](#)]
36. Irving, H.M.N.H.; Khopkar, P.K. The stability of the chloride complexes of europium. *J. Inorg. Nucl. Chem.* **1964**, *26*, 1561–1569. [[CrossRef](#)]
37. Marcus, Y. Anion exchange of metal complexes—XV: Anion exchange and amine extraction of lanthanides and trivalent actinides from chloride solutions. *J. Inorg. Nucl. Chem.* **1966**, *28*, 209–219. [[CrossRef](#)]
38. Breen, P.J.; Horrocks, W.D.W.J. Europium(III) luminescence excitation spectroscopy. Inner-sphere complexation of europium(III) by chloride, thiocyanate, and nitrate ions. *Inorg. Chem.* **1983**, *22*, 536–540. [[CrossRef](#)]
39. Bünzli, J.C.G.; Yersin, J.R. Fluorescence spectra and lifetime measurements of aqueous solutions of europium nitrate and perchlorate. *Inorg. Chem.* **1979**, *18*, 605–607. [[CrossRef](#)]
40. Gorbunov, A.O.; Lindqvist-Reis, P.; Mereshchenko, A.S.; Skripkin, M.Y. Solvation and complexation of europium(III) ions in triflate and chloride aqueous-organic solutions by TRLF spectroscopy. *J. Mol. Liquids* **2017**, *240*, 25–34. [[CrossRef](#)]
41. Reuben, J.; Fiat, D. Nuclear Magnetic Resonance Studies of Solutions of the Rare-Earth Ions and Their Complexes. III. Oxygen-17 and Proton Shifts in Aqueous Solutions and the Nature of Aquo and Mixed Complexes. *J. Chem. Phys.* **1969**, *51*, 4909–4917. [[CrossRef](#)]
42. Chen, Z.; Detellier, C. Interactions of La(III) with anions in aqueous solutions. A <sup>139</sup>La NMR study. *J. Sol. Chem.* **1992**, *21*, 941–952. [[CrossRef](#)]
43. Yaita, T.; Ito, D.; Tachimori, S. <sup>139</sup>La NMR Relaxation and Chemical Shift Studies in the Aqueous Nitrate and Chloride Solutions. *J. Phys. Chem. B* **1998**, *102*, 3886–3891. [[CrossRef](#)]
44. Purdie, N.; Vincent, C.A. Ultrasonic absorption in the lanthanide sulphates. *Trans. Faraday Soc.* **1967**, *63*, 2745–2757. [[CrossRef](#)]
45. Fay, D.P.; Litchinsky, D.; Purdie, N. Ultrasonic absorption in aqueous salts of the lanthanides. *J. Phys. Chem.* **1969**, *73*, 544–552. [[CrossRef](#)]
46. Garnsey, R.; Ebdon, D.W. Ionic association in aqueous lanthanide nitrate solutions by ultrasonic absorption spectroscopy. *J. Am. Chem. Soc.* **1969**, *91*, 50–56. [[CrossRef](#)]
47. Voleišienė, B.; Rutkūnienė, D. Investigation of the hydration phenomenon in 3-1 electrolyte solutions. *Ultragarsas* **2007**, *1*, 45–47.
48. Rudolph, W.W.; Mason, R.; Pye, C.C. Aluminium(III) hydration in aqueous solution. A Raman spectroscopic investigation and an *ab initio* molecular orbital study of aluminium(III) water clusters. *Phys. Chem. Chem. Phys.* **2000**, *2*, 5030–5040. [[CrossRef](#)]
49. Rudolph, W.W.; Irmer, G. Raman and Infrared Spectroscopic Investigations on Aqueous Alkali Metal Phosphate Solutions and Density Functional Theory Calculations of Phosphate—Water Clusters. *Appl. Spectrosc.* **2007**, *61*, 1312–1327. [[CrossRef](#)]
50. Rudolph, W.W.; Pye, C.C. Gallium(III) hydration in aqueous solution of perchlorate, nitrate and sulfate. Raman and <sup>71</sup>Ga NMR spectroscopic studies and *ab initio* molecular orbital calculations of gallium(III) water clusters. *Phys. Chem. Chem. Phys.* **2002**, *4*, 4319–4327. [[CrossRef](#)]
51. Rudolph, W.W.; Brooker, M.H.; Pye, C.C. Hydration of Lithium Ion in Aqueous Solutions. *J. Phys. Chem.* **1995**, *99*, 3793–3797. [[CrossRef](#)]
52. Kanno, H. Hydrations of metal ions in aqueous electrolyte solutions: A Raman study. *J. Phys. Chem.* **1988**, *92*, 4232–4236. [[CrossRef](#)]
53. Vogel, A.I. *A Text-Book of Quantitative Inorganic Analysis*, 3rd ed.; Longman: London, UK, 1961.
54. Spedding, F.H.; Jaffe, S. Conductances, Solubilities and Ionization Constants of Some Rare Earth Sulfates in Aqueous Solutions at 25°. *J. Am. Chem. Soc.* **1954**, *76*, 882–884. [[CrossRef](#)]
55. Rudolph, W.W.; Fischer, D.; Irmer, G. Vibrational Spectroscopic Studies and Density Functional Theory Calculations of Speciation in the CO<sub>2</sub>—Water System. *Appl. Spectrosc.* **2006**, *60*, 130–144. [[CrossRef](#)] [[PubMed](#)]
56. Frisch, M.J.; Trucks, G.W.; Schlegel, H.B.; Scuseria, G.E.; Robb, M.A.; Cheeseman, J.R.; Montgomery, J.A.J.T.; Vreven, K.N.; Kudin, J.C.; Burant, J.M.; et al. *Gaussian 03, Revision, C.02*; Gaussian, Inc.: Wallingford, CT, USA, 2004.
57. Lee, C.; Yang, W.; Parr, R.C. Development of the Colle-Salvetti correlation-energy formula into a functional of the electron density. *Phys. Rev. B* **1988**, *37*, 785–789. [[CrossRef](#)]

58. Cossi, M.; Scalmani, G.; Rega, N.; Barone, V. New developments in the polarizable continuum model for quantum mechanical and classical calculations on molecules in solution. *J. Chem. Phys.* **2002**, *117*, 43–54. [[CrossRef](#)]
59. Smith, D.W. Ionic hydration enthalpies. *J. Chem. Educ.* **1977**, *54*, 540–542. [[CrossRef](#)]
60. Marcus, Y. A simple empirical model describing the thermodynamics of hydration of ions of widely varying charges, sizes, and shapes. *Biophys. Chem.* **1994**, *51*, 111–127. [[CrossRef](#)]
61. Burgess, J. *Ions in Solution: Basic Principles of Chemical Interactions*; Ellis, H., Ed.; Chichester/Halsted Press: New York, NY, USA, 1988.
62. Rudolph, W.; Schönherr, S. Raman- und Infrarotspektroskopische Untersuchungen an konzentrierten Aluminiumsalzlösungen. *Z. Phys. Chem.* **1989**, *270*, 1121–1134. [[CrossRef](#)]
63. Pearson, R.G. Hard and Soft Acids and Bases. *J. Am. Chem. Soc.* **1963**, *85*, 3533–3539. [[CrossRef](#)]
64. Rao, L.; Tian, G. Complexation of Lanthanides with Nitrate at Variable Temperatures: Thermodynamics and Coordination Modes. *Inorg. Chem.* **2009**, *48*, 964–970. [[CrossRef](#)] [[PubMed](#)]
65. Rudolph, W.W.; Irmer, G.; Hefter, G. Raman spectroscopic investigation of speciation in  $\text{MgSO}_4(\text{aq})$ . *Phys. Chem. Chem. Phys.* **2003**, *5*, 5253–5261. [[CrossRef](#)]
66. Klinkhammer, C.; Böhm, F.; Sharma, V.; Schwaab, G.; Seitz, M.; Havenith, M. Anion dependent ion pairing in concentrated ytterbium halide solutions. *J. Chem. Phys.* **2018**, *148*, 222802. [[CrossRef](#)] [[PubMed](#)]
67. Debye, P. *Polare Molekeln*; S. Hirzel-Verlag: Leipzig, Germany, 1929.
68. Clark, A.E. Density Functional and Basis Set Dependence of Hydrated Ln(III) Properties. *J. Chem. Theory Comput.* **2008**, *4*, 708–718. [[CrossRef](#)] [[PubMed](#)]

**Sample Availability:** Samples of  $\text{Lu}(\text{ClO}_4)_3(\text{aq})$  and Lu(III)-triflate(cr) are available in small quantities from the authors. All other solutions have been used.



© 2018 by the authors. Licensee MDPI, Basel, Switzerland. This article is an open access article distributed under the terms and conditions of the Creative Commons Attribution (CC BY) license (<http://creativecommons.org/licenses/by/4.0/>).